

## THE UCSD HIRES/KECK I DAMPED Ly $\alpha$ ABUNDANCE DATABASE:<sup>1</sup> IV. PROBING GALACTIC ENRICHMENT HISTORIES WITH NITROGEN

JASON X. PROCHASKA<sup>2,3</sup>

The Observatories of the Carnegie Institute of Washington  
813 Santa Barbara St.  
Pasadena, CA 91101  
xavier@ociw.edu

AND

RICHARD B.C. HENRY

Department of Physics and Astronomy; University of Oklahoma; Norman, OK 73019  
henry@mail.nhn.ou.edu

AND

JOHN M. O'MEARA<sup>2</sup>, DAVID TYTLER<sup>2</sup>, ARTHUR M. WOLFE<sup>2</sup>, DAVID KIRKMAN<sup>2</sup>,  
DAN LUBIN, & NAO SUZUKI

Department of Physics, and Center for Astrophysics and Space Sciences  
University of California, San Diego; C-0424; La Jolla, CA 92093  
jomeara@ucsd.edu, dtytler@ucsd.edu, awolfe@ucsd.edu, dkirkman@ucsd.edu, dlubin@ucsd.edu, nsuzuki@ucsd.edu  
*Accepted to the Astrophysical Journal: June 14, 2002*

### ABSTRACT

We present 14 N<sup>0</sup> measurements from our HIRES/Keck database of damped Ly $\alpha$  abundances. These data are combined with measurements from the recent and past literature to build an homogeneous, uniform set of observations. We examine photoionization diagnostics like Fe<sup>++</sup> and Ar<sup>0</sup> in the majority of the complete sample and assess the impact of ionization corrections on N/ $\alpha$  and  $\alpha$ /H values derived from observed ionic column densities of N<sup>0</sup>, Si<sup>+</sup>, H<sup>0</sup>, and S<sup>+</sup>. Our final sample of 19 N/ $\alpha$ ,  $\alpha$ /H pairs appears bimodal; the majority of systems show N/ $\alpha$  values consistent with metal-poor emission regions in the local universe but a small sub-sample exhibit significantly lower N/ $\alpha$  ratios. Contrary to previous studies of N/ $\alpha$  in the damped systems, our sample shows little scatter within each sub-sample. We consider various scenarios to explain the presence of the low N/ $\alpha$  sightlines and account for the apparent bimodality. We favor a model where at least some galaxies undergo an initial burst of star formation with suppressed formation of intermediate-mass stars. We found a power-law IMF with slope 0.10 or a mass cut of  $\approx 5 - 8M_{\odot}$  would successfully reproduce the observed LN-DLA values. If the bimodal distribution is confirmed by a larger sample of measurements, this may present the first observational evidence for a top heavy initial mass function in some early stellar populations.

*Subject headings:* galaxies: abundances — galaxies: chemical evolution — quasars : absorption lines — nucleosynthesis

### 1. INTRODUCTION

Abundance studies of the damped Ly $\alpha$  systems – protogalaxies with large H I surface densities  $N(\text{HI}) > 2 \times 10^{20} \text{ cm}^{-2}$  – reveal the chemical enrichment history of the universe. These quasar absorption line systems dominate the neutral hydrogen reservoir to  $z \sim 4$  (Wolfe et al. 1995; Storrie-Lombardi and Wolfe 2000; Peroux et al. 2001) and, therefore, their metal abundances presumably reflect the past and current processes of protogalactic star formation (e.g. Pei et al. 1999). High resolution surveys of the damped systems measure the metal content of these galaxies and trace the evolution in Zn and Fe metallicity with redshift (Pettini et al. 1994; Prochaska & Wolfe 2000). Although these observations track the gross census of metals with time, they only crudely describe the physical processes of metal enrichment. To examine issues related to the initial mass function (IMF), the formation epoch, and the

star formation rate of individual systems, one must pursue other diagnostics.

One important avenue for addressing the details of chemical enrichment is through the investigation of relative metal abundances like O/Fe (e.g. Tinsley 1979). By comparing the so-called  $\alpha$ -elements, elements presumed to form primarily in massive star supernovae, against Fe one roughly assesses the relative contribution of Type Ia and Type II SN which relates to the IMF and star formation history. Although current observations of the damped systems (Prochaska & Wolfe 2002) suggest an  $\alpha$ -enhancement at low metallicity similar to Galactic metal-poor stars (Wheeler et al. 1989; McWilliam 1997), these measurements are subject to the effects of differential depletion (Vladilo 1998; Ledoux, Bergeron, & Petitjean 2002). To date, it has proved a great challenge to isolate the competing effects of nucleosynthesis and differential depletion for ratios like Si/Fe and O/Fe. One can minimize these uncertainties by examining a larger set of  $\alpha$  and Fe-peak elements (e.g. Dessauges-Zavadsky, Prochaska, & D'Odorico 2002a), but this requires extensive observations and is still subject to some uncertainty.

<sup>1</sup> <http://kingpin.ucsd.edu/~hiresdla>

<sup>2</sup> Visiting Astronomer, W.M. Keck Telescope. The Keck Observatory is a joint facility of the University of California and the California Institute of Technology.

<sup>3</sup> Hubble fellow

A complementary approach toward tracing the detailed enrichment history of protogalaxies is to consider the relative abundance of nitrogen. Nitrogen is mainly produced in the six steps of the CN branch of the CNO cycles within H burning stellar zones, where  $^{12}\text{C}$  serves as the reaction catalyst (see a textbook like Clayton 1983 or Cowley 1995 for a nucleosynthesis review). Three reactions occur to transform  $^{12}\text{C}$  to  $^{14}\text{N}$ :  $^{12}\text{C}(\text{p},\gamma)^{13}\text{N}(\beta^+,\nu)^{13}\text{C}(\text{p},\gamma)^{14}\text{N}$ , while the next step,  $^{14}\text{N}(\text{p},\gamma)^{15}\text{O}$ , depletes nitrogen and has a relatively low cross-section. The final two reactions in the cycle transform  $^{15}\text{O}$  to  $^{12}\text{C}$ . Since the fourth reaction runs much slower than the others, the cycle achieves equilibrium only when  $^{14}\text{N}$  accumulates to high levels, and so one effect of the CN cycle is to convert  $^{12}\text{C}$  to  $^{14}\text{N}$ .

One issue in nitrogen evolution is to discover the source of the carbon which is converted into nitrogen, and of any oxygen which can contribute through the (slow) side chain  $^{16}\text{O}(\text{p},\gamma)^{17}\text{F}(\beta^+,\nu)^{17}\text{O}(\text{p},\alpha)^{14}\text{N}$ . For example, stars may produce their own carbon (and some oxygen) during helium burning, and the carbon (and perhaps oxygen) is subsequently processed into  $^{14}\text{N}$  via the CN(O) cycle. In this case, nitrogen production is independent of the initial composition of the star in which it is synthesized and is referred to as *primary* nitrogen. On the other hand, stars beyond the first generation in a galactic system already contain some carbon and oxygen, inherited from the interstellar medium out of which they formed. The amount of nitrogen formed from CNO cycling of this material will then be proportional to its C abundance (and also its O abundance, if the CNO cycling proceeds long enough to deplete the oxygen) and is known as *secondary* nitrogen. To zeroth order, then, primary nitrogen production is independent of metallicity, while secondary production is linearly proportional to metallicity. The effects of metallicity on nitrogen production is one facet of nitrogen evolution we would like to understand clearly.

A second issue of concern in the origin of nitrogen is to identify the portion of the stellar mass spectrum which is most responsible for  $^{14}\text{N}$  production. While only massive stars ( $M > 8M_{\odot}$ ) can produce the necessary internal temperatures required to synthesize most heavy elements, in the case of nitrogen intermediate-mass stars (IMS;  $1-8M_{\odot}$ ) are also massive enough to attain required temperatures for its synthesis. In fact, both observational evidence and theoretical predictions strongly indicate that significant amounts of nitrogen are produced in intermediate-mass stars ( $M < 8M_{\odot}$ ), while some is also synthesized in massive stars (Maeder 1992; Woosley & Weaver 1995; van den Hoek & Groenewegen 1997; Henry, Kwitter, & Bates 2000; Henry, Edmunds, & Köppen 2000, hereafter HEK00; Marigo 2001; Meynet & Maeder 2002; Siess, Livio, & Lattanzio 2002). And since the timescale for IMS evolution is longer than for massive stars, nitrogen production and ejection into the interstellar medium may be significantly delayed with respect to oxygen and other heavy elements that are produced primarily in massive stars. This in turn means that nitrogen evolution is affected by the form of the initial mass function (IMF), time dependence of the star formation rate, and the effective stellar nitrogen yields of both massive and intermediate-mass stars.

Local measurements of emission line regions have examined the abundance of nitrogen relative to O and other  $\alpha$ -

elements as a function of metallicity (see Henry & Worthey 2000 for a compilation). These observations have provided evidence for the contributions of both the primary and secondary nitrogen mechanisms described above to the cosmic abundance evolution of this element. For example, one observes (i) a 'plateau' of  $\text{N}/\alpha$  measurements at  $[\alpha/\text{H}] < -1$  consistent with primary nitrogen formation, i.e., independent of metallicity; and (ii) a rise in  $\text{N}/\alpha$  with increasing metallicity above  $[\alpha/\text{H}] \approx -1$  suggestive of secondary nitrogen formation. Similar observations can be performed with the damped  $\text{Ly}\alpha$  systems (Pettini et al. 1995; Lu et al. 1998, hereafter L98; Centurión et al. 1998). Because damped systems tend to have low metallicity ( $Z < Z_{\odot}/10$ ) their  $\text{N}/\alpha$  measurements probe the primary regime of nitrogen production. In addition, since these systems are relatively young and may not have achieved a stage of steady evolution because of differences in stellar evolution time scales over the stellar mass spectrum,  $\text{N}/\alpha$  may allow us to gauge the effects of time delay and the role of IMS in nitrogen production. And unlike the  $\alpha/\text{Fe}$  ratios described above, the  $\text{N}/\alpha$  observations are largely free of the uncertainties due to differential depletion because of the mild refractory nature of N, O, S, and Si. In fact the most significant source of uncertainty is due to the effects of photoionization: measurements of ions  $\text{N}^0$ ,  $\text{O}^0$ ,  $\text{S}^+$ ,  $\text{H}^0$ , and  $\text{Si}^+$  must be converted to elemental abundances.

The initial studies of  $\text{N}/\alpha$  in damped systems suggested a significant scatter in the  $\text{N}/\alpha$  ratios (L98) with a few systems showing values below the plateau defined by low metallicity H II regions. These observations are difficult to interpret as either purely primary or secondary nitrogen formation and a combination of the two channels was suggested (L98). In this paper, we will reexamine these conclusions. We present 14 nitrogen measurements from our UCSD HIRES/Keck I damped  $\text{Ly}\alpha$  database (Prochaska et al. 2001; hereafter, P01). and combine these data with six from previous studies and an additional five measurements from the recent literature. We restrict our discussion to high resolution echelle observations because (1) the NI transitions lie within the  $\text{Ly}\alpha$  forest where line-blending is important; (2) several NI transitions are subject to line saturation; and (3) the NI 1134 and 1200 triplets are very closely spaced. We limit the analysis to the damped  $\text{Ly}\alpha$  systems where the effects of photoionization are more likely to be small. We synthesize the abundance measurements from these various studies, investigate the effects of photoionization, and present a homogeneous, uniform sample of  $\text{N}/\alpha$  and  $\alpha/\text{H}$  measurements. We then consider various models of N production and describe the implications for the star formation histories within the damped  $\text{Ly}\alpha$  systems.

## 2. THE UCSD HIRES DATABASE

All of the systems comprising the UCSD database were observed on the Keck I telescope with the HIRES spectrograph (Vogt et al. 1994). Most of the observations are described in P01 and we refer the reader to that paper for more details on the acquisition and processing of the data. For several of the systems presented in this section, we also rely upon measurements made with the UVES spectrograph (Dekker et al. 2000) on the VLT. In the following subsections, we present the nitrogen transitions as

well as other transitions relevant to our analysis. These include intermediate-ion transitions like Fe III 1122 which help reveal the ionization state of the gas and  $\alpha$ -element transitions like Si II 1808 which are essential for assessing the enrichment history. The following sub-sections present the figures and ionic column density measurements for each system. For ions with multiple transitions measured, we report the variance-weighted mean. Table 1 lists the atomic data adopted throughout the paper where column 2 lists the rest wavelength, column 3 gives the oscillator strength, and column 4 lists the reference. Complete abundance measurements made from the new observations will be provided in our abundance database<sup>4</sup>.

TABLE 1  
ATOMIC DATA

Transition	$\lambda$	$f$	Ref
O I 976	976.4481	0.00330000	1
N III 989	989.7990	0.10660000	1
Si II 989	989.8731	0.13300000	1
S III 1012	1012.5020	0.03550000	1
O I 1039	1039.2304	0.00919700	1
Ar I 1048	1048.2199	0.26280000	3
Fe II 1063	1063.1760	0.06000000	1
Fe II 1064	1063.9718	0.00371800	2
Ar I 1066	1066.6600	0.06747000	3
N II 1083	1083.9900	0.10310000	1
Fe II 1121	1121.9748	0.02020000	2
Fe III 1122	1122.5260	0.16200000	3
NI 1134	1134.1653	0.01342000	1
NI 1134	1134.4149	0.02683000	1
NI 1134	1134.9803	0.04023000	1
Fe II 1143	1143.2260	0.01770000	2
Fe II 1144	1144.9379	0.10600000	2
S III 1190	1190.2080	0.02217000	1
Si II 1190	1190.4158	0.25020000	1
Si III 1193	1193.2897	0.49910000	1
NI 1199	1199.5496	0.13000000	1
NI 1200	1200.2233	0.08620000	1
NI 1200	1200.7098	0.04300000	1
Si III 1206	1206.5000	1.66000000	1
HI-A 1215	1215.6701	0.41640000	1
S II 1250	1250.5840	0.00545300	1
S II 1253	1253.8110	0.01088000	1
S II 1259	1259.5190	0.01624000	1
O I 1302	1302.1685	0.04887000	1
Si II 1304	1304.3702	0.09400000	4
Al III 1670	1670.7874	1.88000000	1
Si II 1808	1808.0130	0.00218600	11
Al III 1854	1854.7164	0.53900000	1
Al III 1862	1862.7895	0.26800000	1

References. — Key to References – 1: Morton (1991);  
2: Howk et al. (2000); 3: Morton (2002);  
4: Tripp et al. (1996); 11: Bergeson & Lawler (1993)

With few exceptions, we calculate ionic column densities with the same procedures as described in P01, i.e., we implement the apparent optical depth method (Savage and Sembach 1991) for the majority of measurements. This technique, however, cannot be applied to transitions where line-blending or saturation is significant. This occurs more frequently for transitions presented in this paper because the majority arise within the Ly $\alpha$  forest. For these cases, we either present upper limits on the measured column

densities or have performed a full line-profile analysis with the VPFIT software package kindly provided by R. Carswell and J. Webb. Note that the tables report [X/H] measurements for the low-ion species having adopted the meteoritic solar abundances from Grevesse et al. (1996) except for N and Ar where we adopt their photometric values and O where we adopt the revised value from Holweger (2001).

### 2.1. PH957, $z = 2.309$

Although this system is included in the UCSD/HIRES database, our observations do not cover the NI transitions. Therefore, we adopt the measurements of N<sup>0</sup> and several other ions from the UVES observations studied in Dessauges-Zavadsky, Prochaska, & D’Odorico (2002b):  $\log N(\text{N}^0) = 15.03 \pm 0.02$ ,  $\log N(\text{HI}) = 21.37 \pm 0.08$ ,  $\log N(\text{S}^+) = 15.11 \pm 0.01$ .

TABLE 2  
IONIC COLUMN DENSITIES: Q0201+36,  $z = 2.463$

Ion	$\lambda$	AODM	$N_{\text{adopt}}$	[X/H]
HI	1215.7	$20.380 \pm 0.045$		
N I	1134.1		$> 15.000$	$> -1.350$
N II	1083.9	$> 15.303$		
Si II			$15.532 \pm 0.010$	$-0.408 \pm 0.046$
S II	1253.8	$15.287 \pm 0.011$	$15.287 \pm 0.011$	$-0.293 \pm 0.046$
Ar I	1048.2	$14.077 \pm 0.030$	$14.077 \pm 0.030$	$-0.823 \pm 0.054$
Fe II			$15.008 \pm 0.004$	$-0.872 \pm 0.045$
Fe III	1122.5	$13.855 \pm 0.023$		

### 2.2. Q0201+36, $z = 2.463$

We present a series of metal-line profiles for this damped system in Figure 1 including NI, Fe III, and Ar I. Because the velocity profiles extend over 200 km/s, the two NI triplets are significantly self-blended. To estimate the N<sup>0</sup> column density, we have performed a line-profile analysis of these transitions with the VPFIT software package. Unfortunately, the blending is so severe and complicated that we could not achieve a satisfactory solution. In turn, we can only place a very conservative lower limit of  $N(\text{N}^0) > 10^{15} \text{ cm}^{-2}$ . Note, the  $N(\text{Fe}^{++})$  value listed in Table 2 refers to the velocity region  $-120 \text{ km s}^{-1} < v < 40 \text{ km s}^{-1}$  which does not include the strong feature at  $v \approx -150 \text{ km s}^{-1}$ , a probable line-blend. Similarly, we report an  $N(\text{Fe}^+)$  value corresponding to the same velocity region to enable an evaluation of the  $\text{Fe}^{++}/\text{Fe}^+$  ratio (§ 3).

### 2.3. Q0336-01, $z = 3.062$

Figure 2 presents the NI transitions observed for the damped Ly $\alpha$  system at  $z = 3.062$  toward Q0336-01. Unfortunately all of the NI profiles are at least partially saturated and we can only set a lower limit on the N<sup>0</sup> column density. Table 3 lists the ionic column density measurements and the variance-weighted means. From Fe III 1122, we report an upper limit to  $N(\text{Fe}^{++})$  because of the presence of a significant line blend at  $v > 0 \text{ km s}^{-1}$ . Similarly, we classify our  $N(\text{N}^+)$  measurement as an upper limit because we suspect line-blending with the Ly $\alpha$  forest.

<sup>4</sup> <http://kingpin.ucsd.edu/~hiresdla>

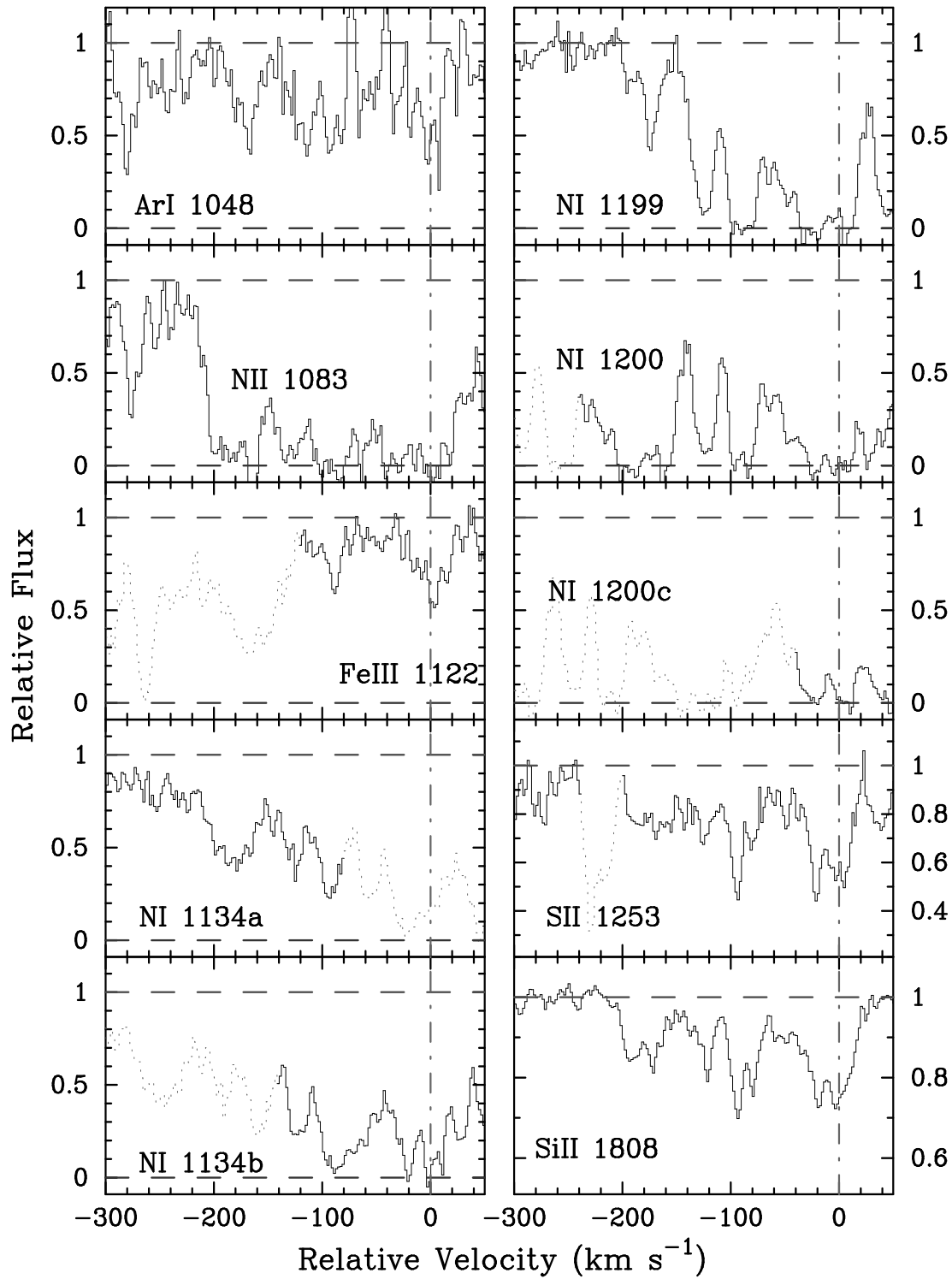


FIG. 1.— Velocity plot of NI and intermediate-ion transitions for the damped  $\text{Ly}\alpha$  system at  $z = 2.463$  toward Q0201+36. For comparison, we also plot the Si II 1808 profile. The vertical line at  $v = 0$  corresponds to  $z = 2.4628$ .

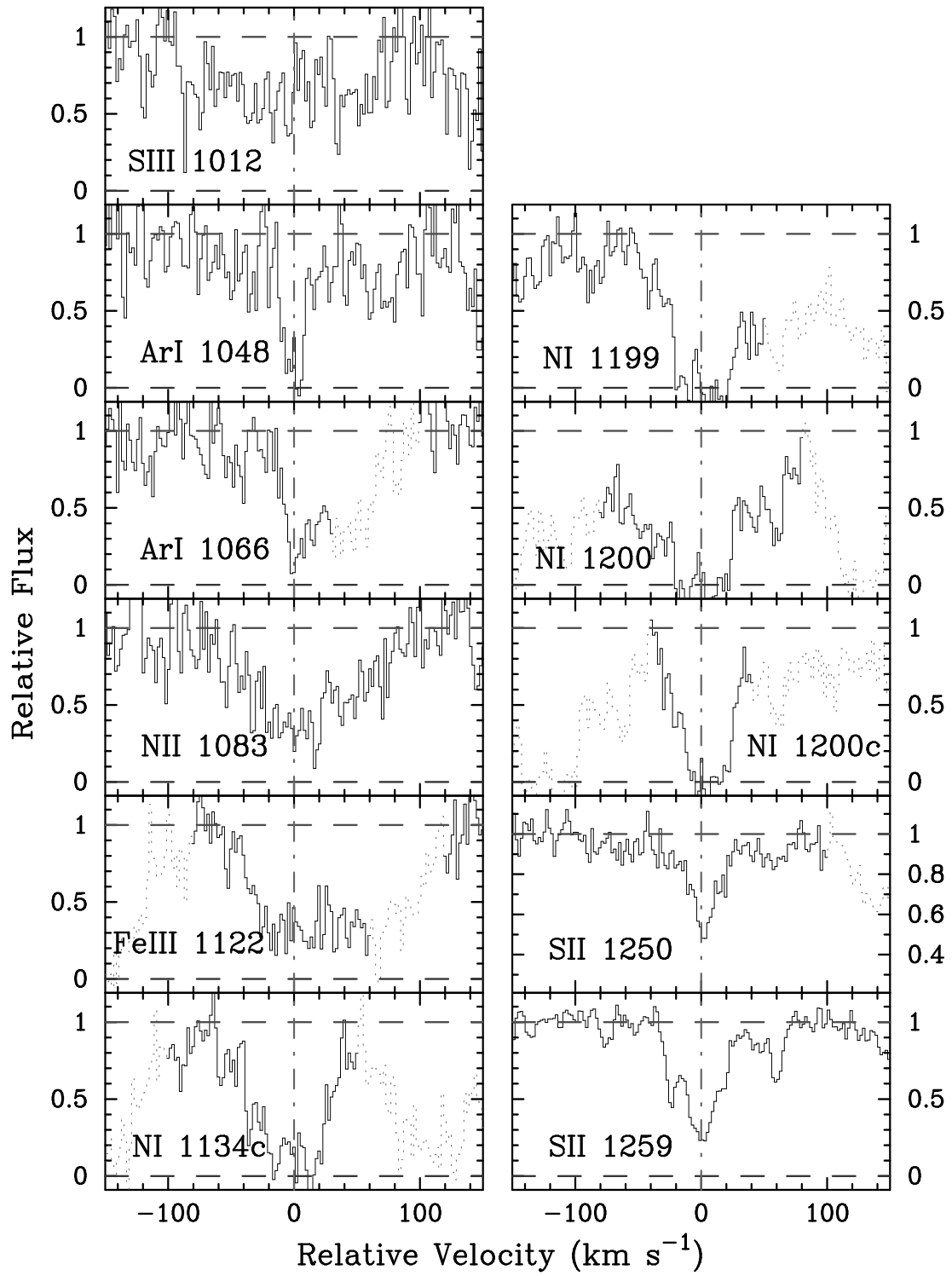


FIG. 2.— Velocity plot of the metal-line transitions for the damped Ly $\alpha$  system at  $z = 3.062$  toward Q0336-01. The vertical line at  $v = 0$  corresponds to  $z = 3.062078$ .

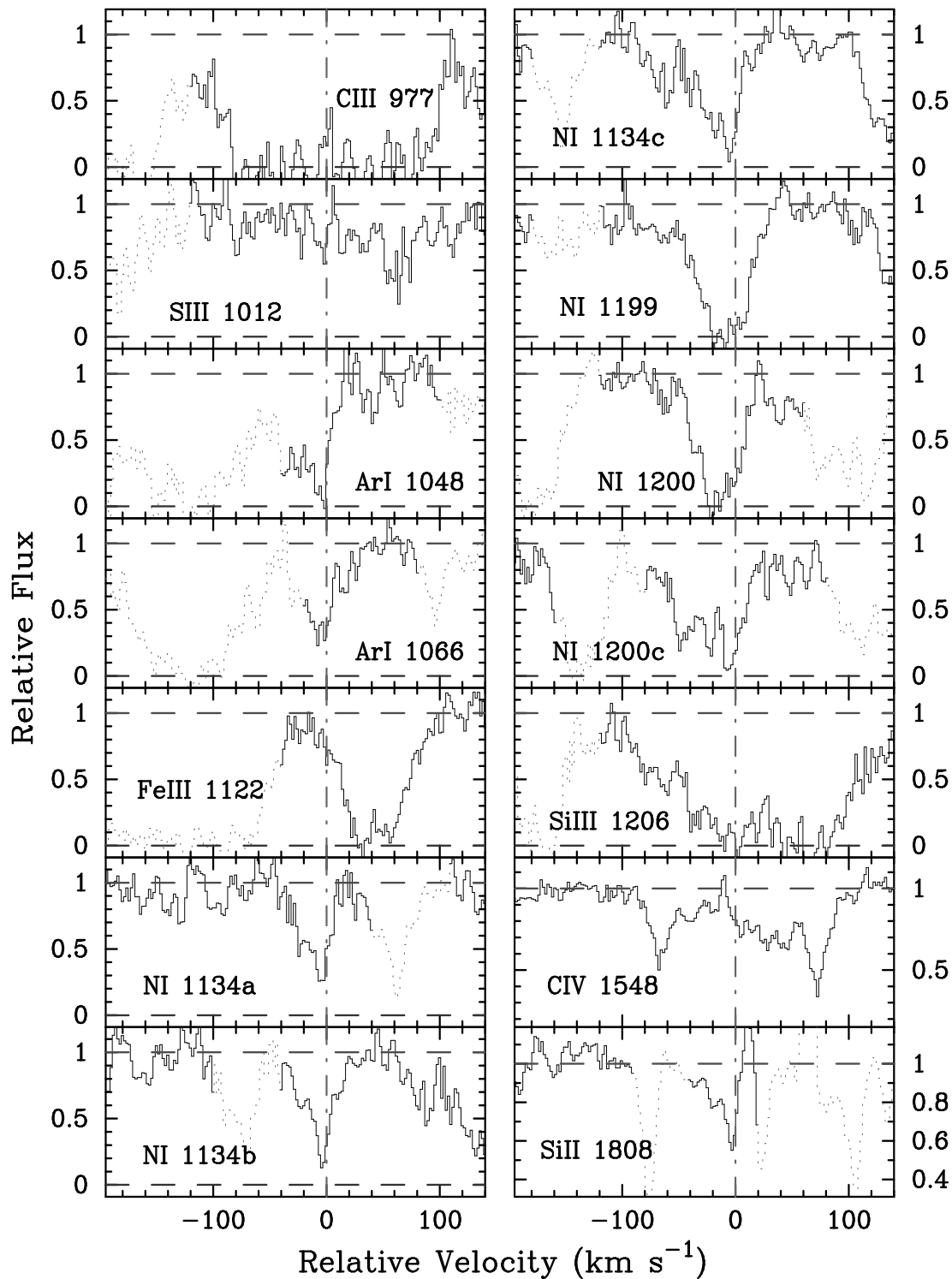


FIG. 3.— Velocity plot of the metal-line transitions for the damped  $\text{Ly}\alpha$  system at  $z = 3.025$  toward Q0347–38. The vertical line at  $v = 0$  corresponds to  $z = 3.0247$ .

TABLE 3

IONIC COLUMN DENSITIES: Q0336-01,  $z = 3.062$ 

Ion	$\lambda$	AODM	$N_{\text{adopt}}$	[X/H]
HI	1215.7	$21.200 \pm 0.100$		
N I	1134.9	$> 15.037$	$> 15.037$	$> -2.133$
N I	1200.7	$> 15.014$		
N II	1083.9	$< 14.371$		
S II	1250.5	$15.118 \pm 0.022$	$14.994 \pm 0.011$	$-1.406 \pm 0.101$
S II	1259.5	$14.970 \pm 0.012$		
S III	1012.5	$< 14.650$	$14.994 \pm 0.011$	$-1.406 \pm 0.101$
Ar I	1048.2	$> 13.939$	$> 13.939$	$> -1.781$
Fe II			$14.905 \pm 0.033$	$-1.795 \pm 0.105$
Fe III	1122.5	$< 14.238$		

TABLE 4

IONIC COLUMN DENSITIES: Q0347-38,  $z = 3.025$ 

Ion	$\lambda$	AODM	$N_{\text{adopt}}$	[X/H]
HI	1215.7	$20.626 \pm 0.005$		
C III	977.0	$> 14.385$		
N I			$14.890 \pm 0.031$	$-1.706 \pm 0.031$
Si II	1808.0	$15.016 \pm 0.026$	$15.016 \pm 0.026$	$-1.170 \pm 0.026$
Si III	1206.5	$> 13.447$		
S II			$< 14.760$	$< -1.066$
S III	1012.5	$13.849 \pm 0.123$		
Ar I	1048.2	$> 14.031$	$14.276 \pm 0.035$	$-0.870 \pm 0.035$
Ar I	1066.6	$14.276 \pm 0.035$		
Fe II			$14.503 \pm 0.007$	$-1.623 \pm 0.009$
Fe III	1122.5	$13.140 \pm 0.080$		

2.4. Q0347-38,  $z = 3.025$ 

The ionic transitions for the damped system toward Q0347-38 are presented in Figure 3. This damped system has been carefully analysed by several authors including Levshakov et al. (2002) who analysed the high quality UVES/VLT commissioning data of this quasar. In the following, we will adopt their HI measurement of  $\log N(\text{HI}) = 20.626 \pm 0.005$  and implement our own metal-line analysis except for nitrogen. The UVES observations include many more NI transitions than our own and have significantly higher S/N ratio. We stress that the  $N(\text{Si}^+)$  value that we have measured is  $\approx 0.25$  dex lower than the value listed in Levshakov et al. (2002). We believe the difference is due to a significant telluric line-blend in the UVES spectrum. Finally, the  $\text{Fe}^{++}$  column density reported in Table 4 refers to the velocity region  $-20 \text{ km s}^{-1} < v < 20 \text{ km s}^{-1}$  and may be considered an upper limit because of the likelihood of blending with neighboring, coincident absorption features.

2.5. HS0741+47,  $z = 3.017$ 

The metal-line profiles for this damped system are shown in Figure 4 which includes NI, SiII, FeIII, NII, and Ar I transitions. Because we expect the Fe III 1122 and N II 1083 profiles are dominated by blends with coincident Ly $\alpha$  clouds, we report their column densities as upper limits (Table 5). These limits were derived by integrating the velocity profiles over the velocity intervals  $-20 \text{ km s}^{-1} < v < 30 \text{ km s}^{-1}$  and  $-40 \text{ km s}^{-1} < v < 20 \text{ km s}^{-1}$  respectively.

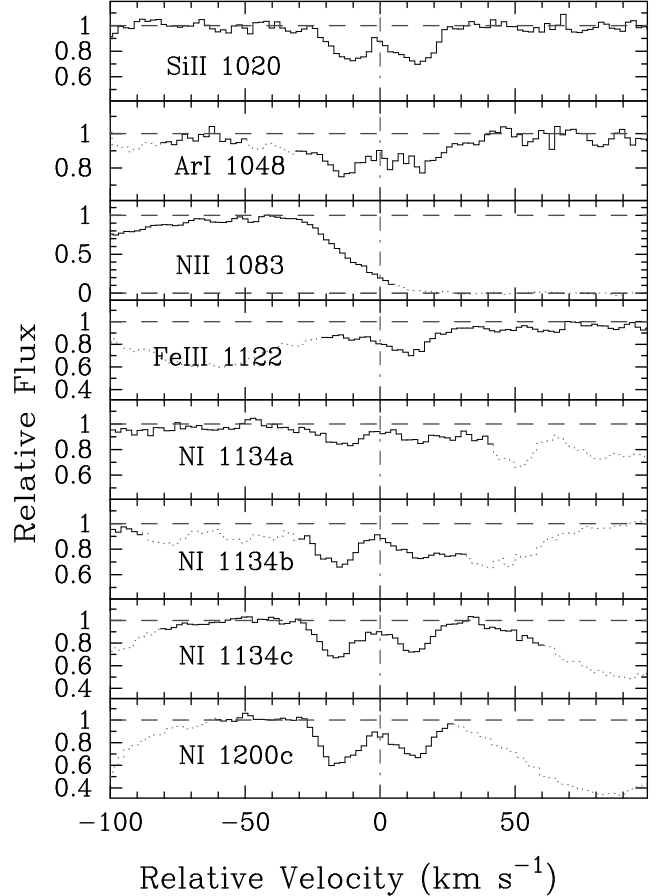
2.6. Q0930+28,  $z = 3.235$ 

FIG. 4.— Velocity plot of the metal-line transitions for the damped Ly $\alpha$  system at  $z = 3.017$  toward HS0741+47. The vertical line at  $v = 0$  corresponds to  $z = 3.017399$ .

TABLE 5

IONIC COLUMN DENSITIES: HS0741+4741,  $z = 3.017$ 

Ion	$\lambda$	AODM	$N_{\text{adopt}}$	[X/H]
HI	1215.7	$20.480 \pm 0.100$		
N I	1134.4	$14.158 \pm 0.015$	$13.977 \pm 0.010$	$-2.473 \pm 0.100$
N I	1134.9	$13.926 \pm 0.017$		
N I	1200.7	$14.012 \pm 0.012$		
N II	1083.9	$< 14.498$		
Si II	1020.6	$14.162 \pm 0.019$	$14.354 \pm 0.003$	$-1.686 \pm 0.100$
Ar I	1048.2	$13.134 \pm 0.020$	$13.134 \pm 0.020$	$-1.866 \pm 0.102$
Fe II			$14.052 \pm 0.005$	$-1.928 \pm 0.100$
Fe III	1122.5	$< 13.290$		

The nitrogen abundance of this damped system was previously analysed by L98. In their paper, they report an HI column density of  $10^{20.18} \text{ cm}^{-2}$  based on their observations of the Ly $\alpha$  transition. We find the Ly $\alpha$  profile is best fit by two HI absorbers at two redshifts: (1)  $z = 3.234946$ ,  $N(\text{HI}) = 10^{20.3}$ , and (2)  $z = 3.246338$ ,  $N(\text{HI}) = 10^{20.2}$ . We estimate a 0.1 dex error for each of these HI measurements. In the following, we restrict the analysis to the  $z = 3.234946$  damped system because we have significant concerns on the ionization state of the 'sub-DLA'.

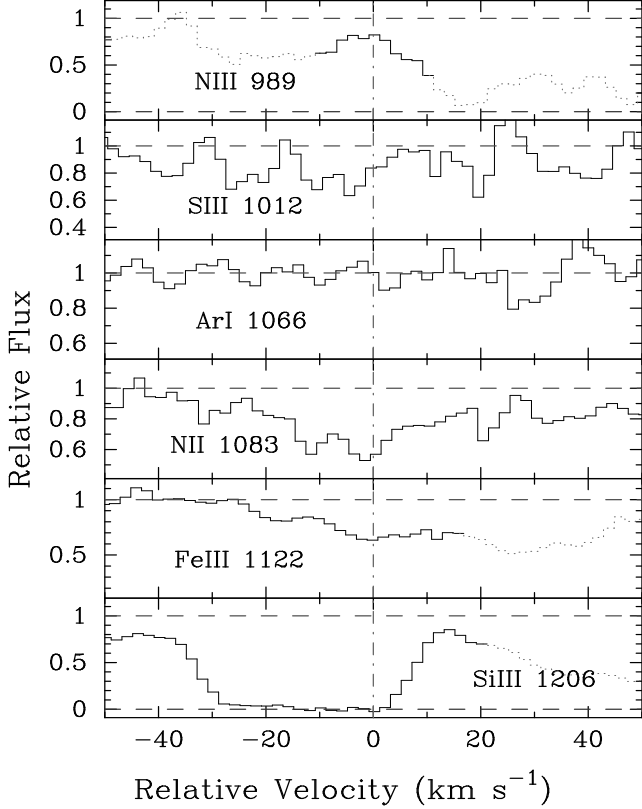


FIG. 5.— Velocity plot of the metal-line transitions for the damped  $\text{Ly}\alpha$  system at  $z = 3.235$  toward Q0930+28. The vertical line at  $v = 0$  corresponds to  $z = 3.2353$ .

TABLE 6

IONIC COLUMN DENSITIES: Q0930+28,  $z = 3.235$

Ion	$\lambda$	AODM	$N_{\text{adopt}}$	[X/H]
HI	1215.7	$20.300 \pm 0.100$		
N I	1134.1	$13.951 \pm 0.057$	$13.740 \pm 0.013$	$-2.530 \pm 0.101$
N I	1199.5	$13.659 \pm 0.022$		
N I	1200.2	$13.762 \pm 0.022$		
N I	1200.7	$13.884 \pm 0.024$		
N II	1083.9	$13.655 \pm 0.033$		
Si II			$13.888 \pm 0.021$	$-1.972 \pm 0.102$
Si III	1206.5	$> 13.481$		
S III	1012.5	$13.837 \pm 0.089$		
Ar I	1066.6	$< 12.960$	$< 12.960$	$< -1.860$
Fe II	1121.9	$13.549 \pm 0.081$	$13.695 \pm 0.015$	$-2.105 \pm 0.101$
Fe II	1144.9	$13.767 \pm 0.032$		
Fe III	1122.5	$13.141 \pm 0.032$		

Figure 5 shows the intermediate-ion and Ar I transitions for this damped system and Table 6 lists the ionic column densities from our and the L98 analysis.

### 2.7. $Q1223+17$ , $z = 2.466$

We reveal the NI, SiII, and FeIII transitions for the damped system toward Q1223+17 in Figure 6. The profiles for this system are spread over 100 km/s such that the members of the NI 1134 triplet are blended with one another. We first estimated the NI column density from this

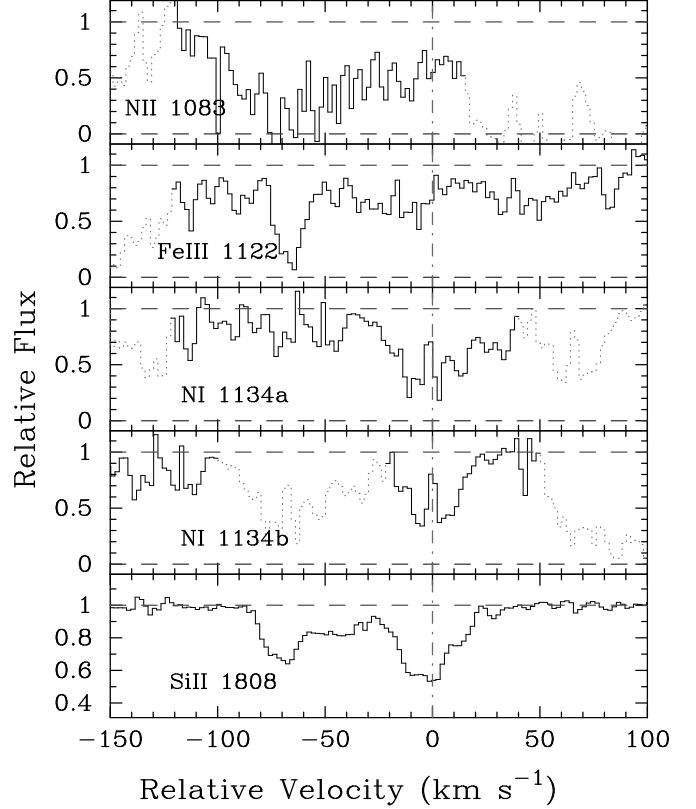


FIG. 6.— Velocity plot of the metal-line transitions for the damped  $\text{Ly}\alpha$  system at  $z = 2.466$  toward Q1223+17. The vertical line at  $v = 0$  corresponds to  $z = 2.466083$ .

TABLE 7

IONIC COLUMN DENSITIES: Q1223+17,  $z = 2.466$

Ion	$\lambda$	AODM	$N_{\text{adopt}}$	[X/H]
HI	1215.7	$21.500 \pm 0.100$		
N I			$14.830 \pm 0.179$	$-2.640 \pm 0.205$
N II	1083.9	$> 14.794$		
Si II			$15.467 \pm 0.008$	$-1.593 \pm 0.100$
Fe II			$15.157 \pm 0.022$	$-1.843 \pm 0.102$
Fe III	1122.5	$< 14.082$		

triplet by integrating the apparent optical depth over all 3 transitions and adopting a summed oscillator strength. We then performed a detailed line-profile analysis of the lines with the VPFIT software package. Unfortunately, at a S/N ratio of 5 we could not constrain the  $N(N^0)$  value to better than 0.2 dex. For this reason, we have chosen to remove it from our analysis.

### 2.8. $Q1331+17$ , $z = 1.776$

Although we adopt the  $\text{Si}^+$  column density presented in P01, we rely on the analysis of Dessauges-Zavadsky, Prochaska, & D'Odorico (2002b) for the majority of measurements considered in this paper. Their UVES-VLT observations cover the NI transitions and intermediate-ions which lie blueward of our wavelength coverage.

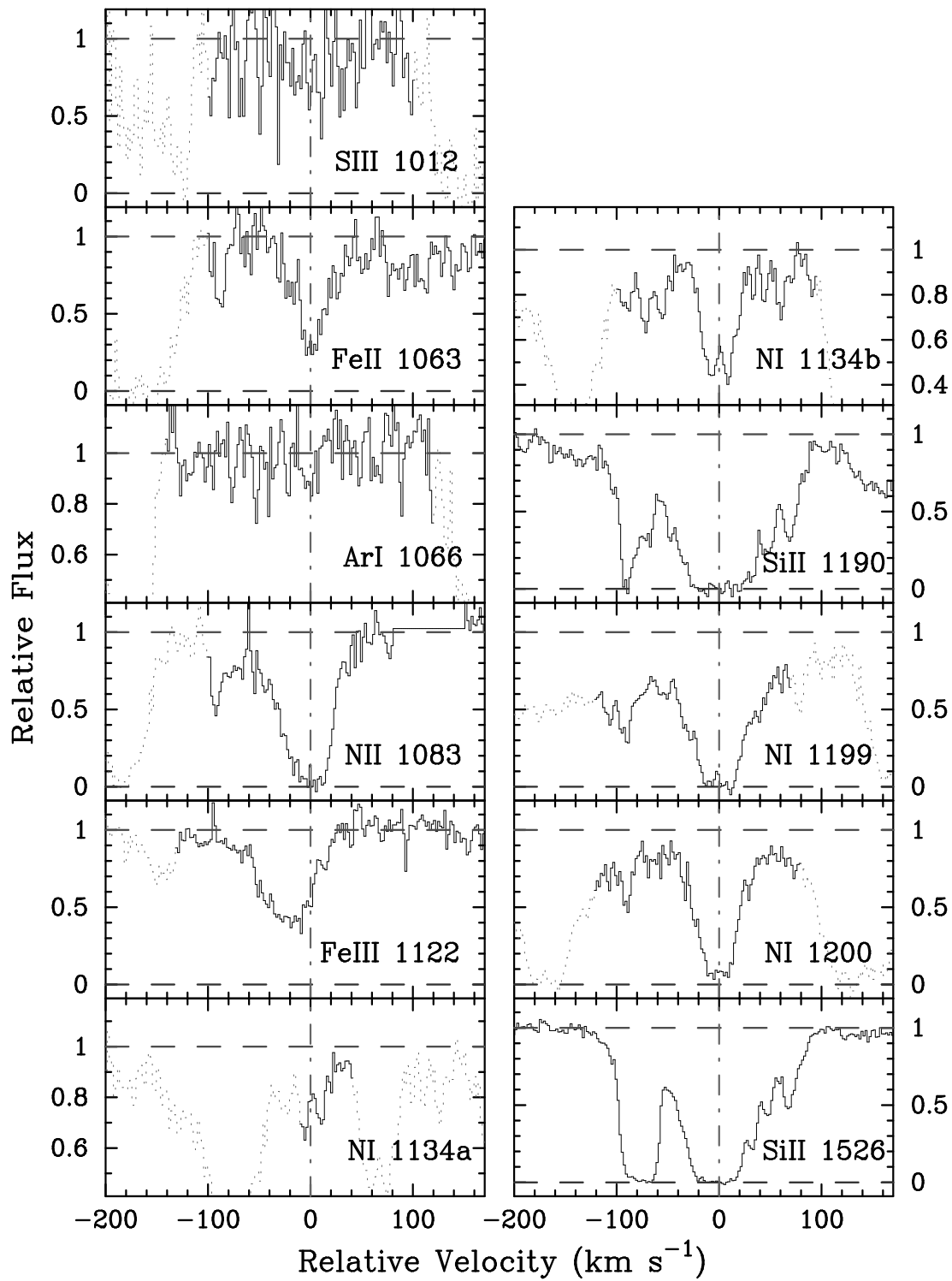


FIG. 7.— Velocity plot of the metal-line transitions for the damped Ly $\alpha$  system at  $z = 2.827$  toward Q1425+60. The vertical line at  $v = 0$  corresponds to  $z = 2.8268$ .

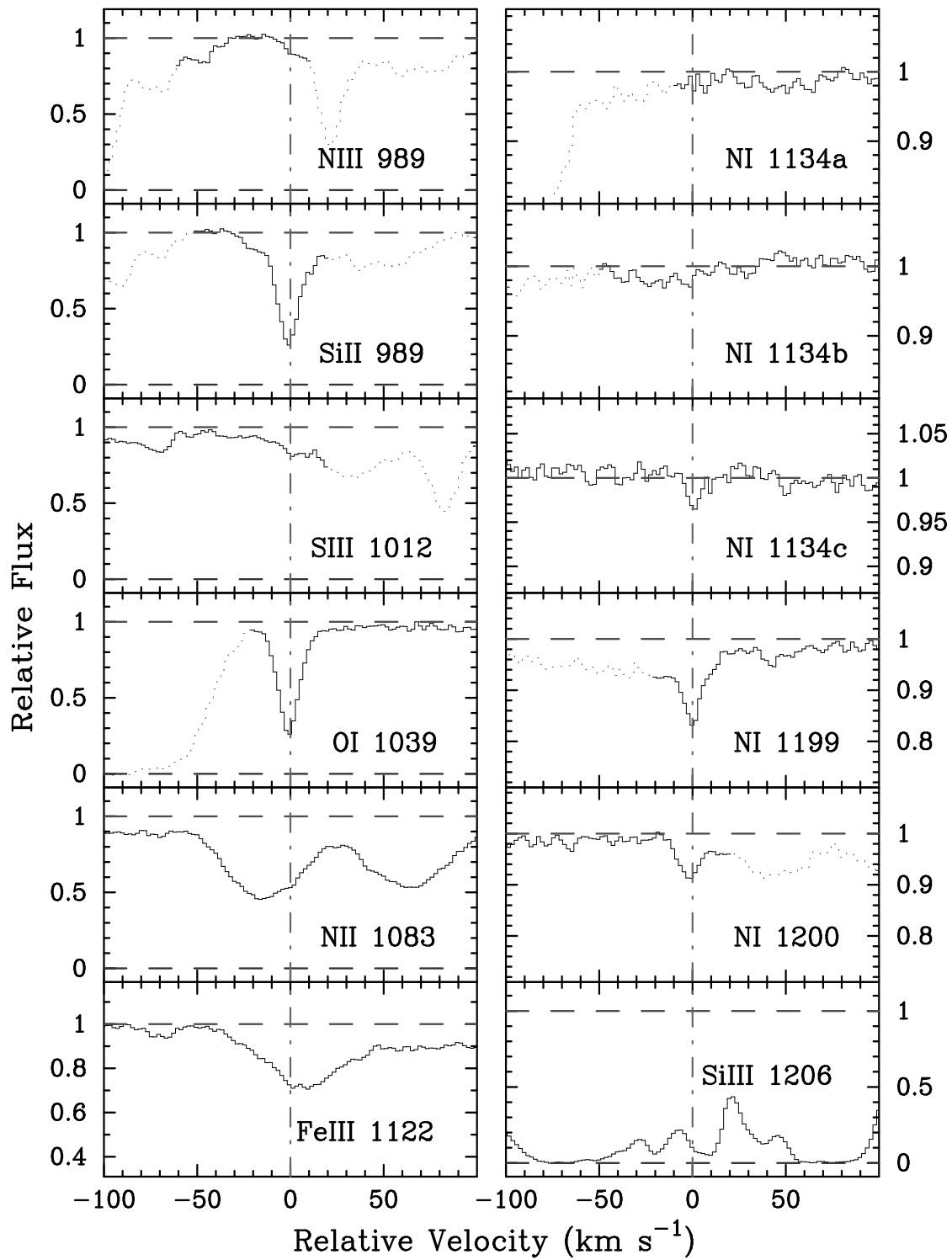


FIG. 8.— Velocity plot of the metal-line transitions for the damped  $\text{Ly}\alpha$  system at  $z = 2.844$  toward Q1946+76. The vertical line at  $v = 0$  corresponds to  $z = 2.8443$ .

TABLE 8

IONIC COLUMN DENSITIES: Q1425+6039,  $z = 2.827$ 

Ion	$\lambda$	AODM	$N_{\text{adopt}}$	[X/H]
HI	1215.7	$20.300 \pm 0.040$		
N I	1134.4	$14.707 \pm 0.014$	$14.707 \pm 0.014$	$-1.563 \pm 0.042$
N I	1200.2	$> 14.623$		
N II	1083.9	$> 14.715$		
Si II	1190.4	$> 14.751$	$> 14.826$	$> -1.034$
Si II	1526.7	$> 14.826$		
S III	1012.5	$14.157 \pm 0.108$		
Ar I	1066.6	$< 13.426$	$< 13.426$	$< -1.394$
Fe II	1143.2	$14.255 \pm 0.039$	$14.471 \pm 0.006$	$-1.329 \pm 0.040$
Fe III	1122.5	$< 14.018$		

2.9. Q1425+60,  $z = 2.827$ 

L98 presented a lower limit on the  $N^0$  column density based on their HIRES spectra of the NI 1200 triplet. Our independent HIRES observations (Figure 7) provide a measurement of  $N^0$  which includes the NI 1134 triplet as listed in Table 8. Our adopted value is just below their limit and we expect the difference is due to blending in the Ly $\alpha$  forest. We note that the stronger NI transitions exhibit a small but significant feature at  $v \approx -90 \text{ km s}^{-1}$  which is evident in the Si II profiles as well as the N II 1083 profile. On the other hand, we suspect that the Fe III 1122 profile is significantly blended with a coincident Ly $\alpha$  cloud and place an upper limit to  $N(\text{Fe}^{++})$ . Unfortunately, both the L98 and our observations only provide a lower limit to  $\text{Si}^+$  which serves as the  $\alpha$ -element for this system.

2.10. GB1759+75,  $z = 2.625$ 

A detailed analysis of this system, including NI, was presented in (Prochaska et al. 2002, hereafter P02). We refer the reader to that paper for figures and tables.

TABLE 9

IONIC COLUMN DENSITIES: Q1946+7658,  $z = 2.844$ 

Ion	$\lambda$	AODM	$N_{\text{adopt}}$	[X/H]
HI	1215.7	$20.270 \pm 0.060$		
N I	1134.1	$< 13.214$	$12.588 \pm 0.039$	$-3.652 \pm 0.072$
N I	1134.4	$< 12.810$		
N I	1134.9	$12.287 \pm 0.141$		
N I	1199.5	$< 12.860$		
N I	1200.2	$12.673 \pm 0.038$		
N II	1083.9	$13.568 \pm 0.005$		
N III	989.7	$12.688 \pm 0.063$		
O I			$14.820 \pm 0.007$	$-2.320 \pm 0.060$
O I	1039.2	$14.813 \pm 0.008$	$14.820 \pm 0.007$	$-2.320 \pm 0.060$
Si II			$13.604 \pm 0.005$	$-2.226 \pm 0.060$
Si III	1206.5	$12.860 \pm 0.005$		
S III	1012.5	$< 13.476$		
Fe II			$13.242 \pm 0.009$	$-2.528 \pm 0.061$
Fe III	1122.5	$< 13.216$		

2.11. Q1946+76,  $z = 2.844$ 

The nitrogen abundance of this system has been examined in several papers (Lu et al. 1996; L98). Our independent observations (Kirkman & Tytler 1997) imply a value in good agreement with the best of the previous

measurements:  $\log N(\text{N}^0) = 12.58 \pm 0.04$ . In Figure 8, we present the NI transitions as well as several other metal-lines relevant to the system's ionization state and Table 9 summarizes the column density measurements. We report a value for  $N(\text{N}^+)$  based on integrating the blended NII 1083 profile over the velocity region  $-10 \text{ km s}^{-1} < v < 10 \text{ km s}^{-1}$ . Finally, the reported  $\text{Si}^{++}$  value was derived by integrating the SiIII 1206 profile over the velocity interval  $-10 \text{ km s}^{-1} < v < 10 \text{ km s}^{-1}$  and might be considered an upper limit given the likelihood of line-blending.

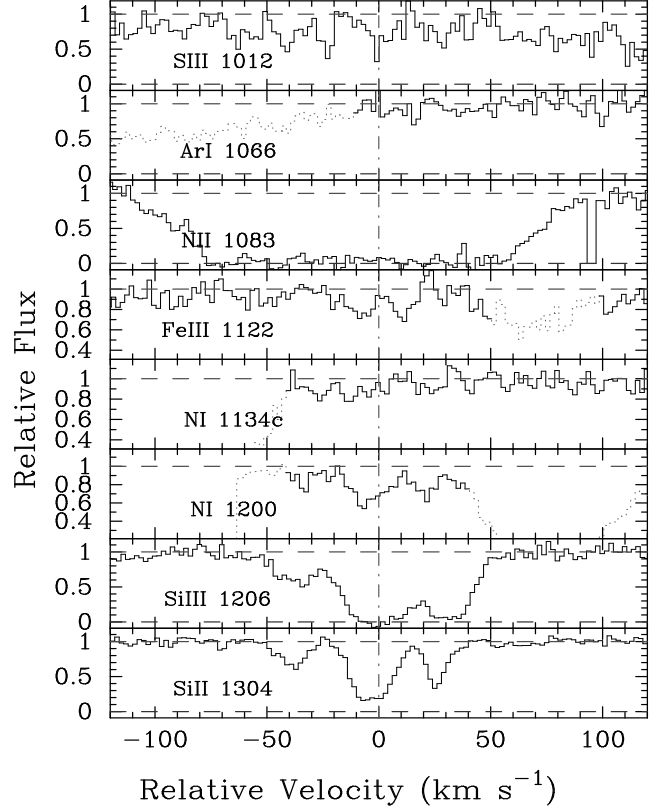


FIG. 9.— Velocity plot of the metal-line transitions for the damped Ly $\alpha$  system at  $z = 2.538$  toward Q2344+12. The vertical line at  $v = 0$  corresponds to  $z = 2.53790$ .

TABLE 10

IONIC COLUMN DENSITIES: Q2344+12,  $z = 2.538$ 

Ion	$\lambda$	AODM	$N_{\text{adopt}}$	[X/H]
HI	1215.7	$20.360 \pm 0.100$		
N I	1134.9	$13.742 \pm 0.088$	$13.779 \pm 0.029$	$-2.551 \pm 0.104$
N I	1200.2	$13.785 \pm 0.031$		
N II	1083.9	$> 15.234$		
Si II			$14.179 \pm 0.012$	$-1.741 \pm 0.101$
Si III	1206.5	$> 13.545$		
S III	1012.5	$14.562 \pm 0.043$		
S III	1190.2	$13.588 \pm 0.089$		
Ar I	1066.6	$< 13.256$	$< 13.256$	$< -1.624$
Fe II			$14.030 \pm 0.032$	$-1.830 \pm 0.105$
Fe III	1122.5	$< 13.229$		

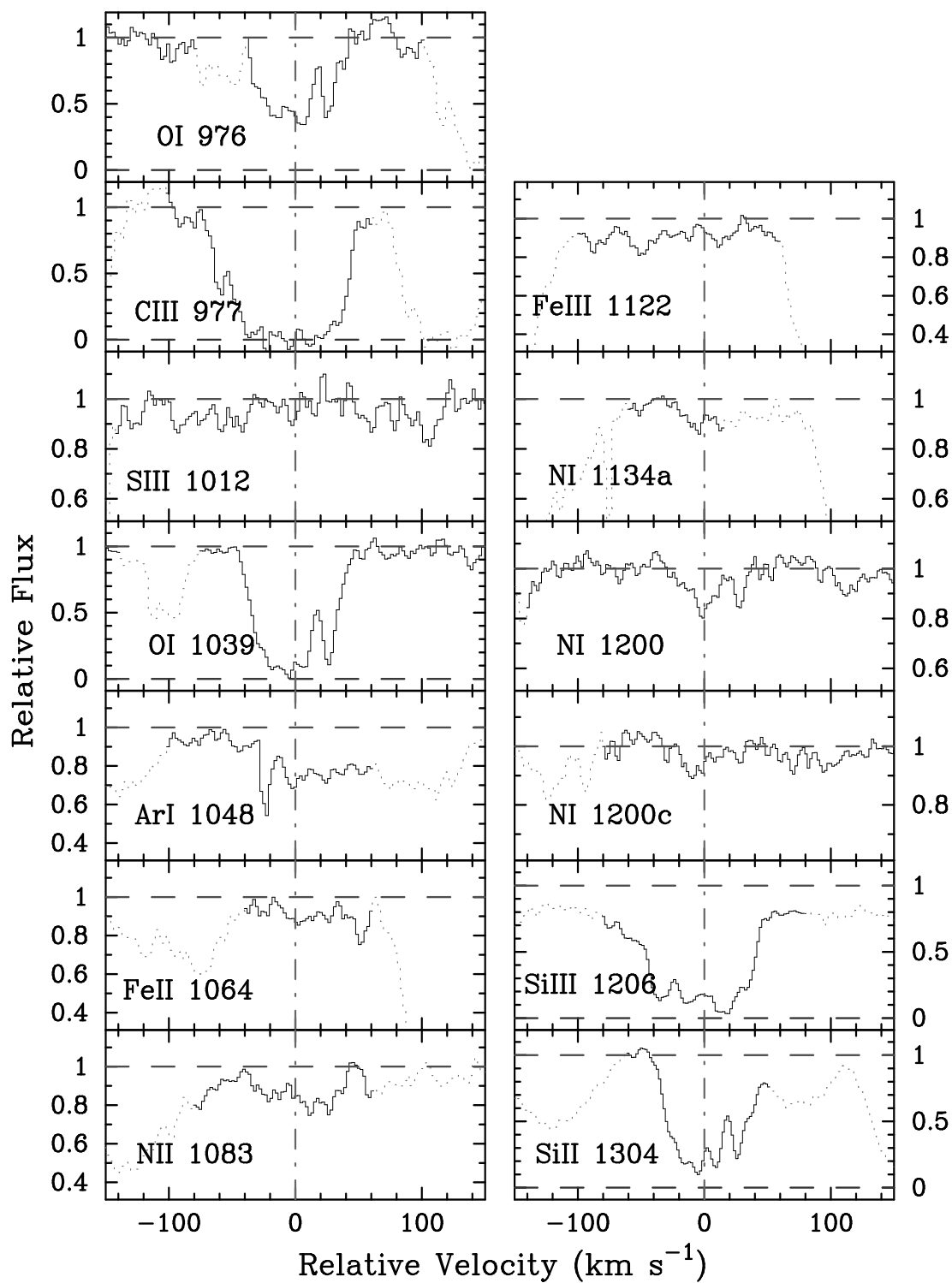


FIG. 10.— Velocity plot of the metal-line transitions for the damped  $\text{Ly}\alpha$  system at  $z = 3$  toward QXO0001.

2.12. *Q2344+12*,  $z = 2.538$ 

L98 presented a measurement of  $N^0$  based on their HIRES observations. Our data covers the same transitions as well as several additional profiles (Figure 9). Unfortunately, the NI 2000a transition is crowded between two Ly $\alpha$  clouds and it is difficult to accurately assess the  $N^0$  column density. Our adopted value,  $N(N^0) = 10^{13.779 \pm 0.03} \text{ cm}^{-2}$ , is  $\approx 0.2$  dex larger than the value reported by L98. This difference is substantial and is probably related to measurements of the continuum level near the NI 1200a profile. Unlike L98, our observations include the NI 1334 triplet and we find an  $N^0$  column density from these lines in good agreement with the NI 1200a transition. Table 10 lists all of the column density measurements related to our  $N/\alpha$  analysis. This includes a reported upper limit to  $N(\text{Fe}^{++})$  where the observed profile is most likely blended with several coincident absorption lines. This conclusion stems from the observed differences between the Fe III 1122 profile and the low-ion transitions, particularly at  $v \approx +5 \text{ km s}^{-1}$ .

TABLE 11

IONIC COLUMN DENSITIES: *Q2348-14*,  $z = 2.279$ 

Ion	$\lambda$	AODM	$N_{\text{adopt}}$	[X/H]
HI	1215.7	$20.560 \pm 0.075$		
N I	1200.2	< 13.235	< 13.235	< -3.295
Al II			$12.657 \pm 0.006$	$-2.393 \pm 0.075$
Al III	1854.7	$12.726 \pm 0.012$		
Al III	1862.7	$12.613 \pm 0.027$		
Si II			$14.203 \pm 0.020$	$-1.917 \pm 0.078$
Si III	1206.5	> 13.499		
S II			$13.725 \pm 0.119$	$-2.035 \pm 0.141$
S III	1190.2	< 13.945		

2.13. *Q2348-14*,  $z = 2.279$ 

Most of the important transitions for this damped Ly $\alpha$  system were presented in Prochaska & Wolfe (1999) including the NI 1200a transition on which our  $N(N^0)$  limit is based. Table 11 lists the column densities taken from that paper with revised oscillator strengths where applicable. We also report an upper limit to  $N(\text{S}^{++})$  based on the partially blended S III 1190 profile.

2.14. *QXO0001*,  $z = 3$ 

Figure 10 presents metal-line profiles for the damped Ly $\alpha$  system at  $z = 3$  toward QXO0001 ( $\log N(\text{HI}) = 20.7 \pm 0.05$ ) which we will discuss further in a future paper. Our observations include several intermediate-ion transitions which we expect are blended with coincident Ly $\alpha$  clouds. Table 12 provides the ionic column density measurements and limits for all of these transitions. Because the Si III 1206 transition arises in one wing of the damped Ly $\alpha$  profile, we first renormalized the continuum surrounding the Si III 1206 profile to account for this depression. The profile is slightly saturated and one may consider our  $N(\text{Si}^{++})$  value to be formally a lower limit.

TABLE 12

IONIC COLUMN DENSITIES: *QXO0001*,  $z = 3$ 

Ion	$\lambda$	AODM	$N_{\text{adopt}}$	[X/H]
HI	1215.7	$20.700 \pm 0.050$		
C III	977.0	> 14.171		
N I	1134.1	< 14.127	$13.315 \pm 0.040$	$-3.355 \pm 0.064$
N I	1200.2	$13.325 \pm 0.043$		
N I	1200.7	$13.272 \pm 0.095$		
N II	1083.9	< 13.637		
N III	989.7	> 14.738		
O I	976.4	$15.766 \pm 0.024$	$15.766 \pm 0.024$	$-1.804 \pm 0.055$
O I	1039.2	> 15.745		
Si II	989.8	> 14.685	$14.452 \pm 0.006$	$-1.808 \pm 0.050$
Si II	1193.2	> 14.280		
Si II	1304.3	$14.453 \pm 0.006$		
Si III	1206.5	$13.47 \pm 0.10$	$13.47 \pm 0.10$	
S III	1012.5	< 13.460		
Ar I	1048.2	< 13.384	< 13.384	< -1.836
Fe II	1063.9	< 15.092	< 15.092	< -1.108
Fe III	1122.5	< 12.965		

3. DETERMINING  $[N/\alpha]$  AND  $[\alpha/H]$ 

The previous section presented all of the systems with observed NI transitions in our HIRES database. For the analysis which follows, we have synthesized these observations with all other high precision nitrogen measurements for damped Ly $\alpha$  systems at  $z > 1.5$ . This includes the important sample introduced by L98, the system toward Q0201+11 by Ellison et al. (2001), and several new measurements (Molaro et al. 2000; Levshakov et al. 2002; Dessauges-Zavadsky, Prochaska, & D’Odorico 2002b; Lopez et al. 2002) obtained with the UVES-VLT spectrograph (Dekker et al. 2000). Table 13 summarizes all of these observations. Column 6 of the table indicates the expected importance of ionization corrections as described below and column 7 indicates whether the system is included in the analysis of § 4. In general, those systems where we expect ionization corrections will be significant but could not reasonably assess their value were eliminated.

Given the appropriate wavelength coverage, high resolution observations of the damped systems can generally provide precise and accurate ionic column densities for both nitrogen and an  $\alpha$ -element. Before converting these gas-phase measurements into elemental abundances and  $N/\alpha$  ratios, however, one must consider several factors: (1) identifying the ‘best’  $\alpha$ -element; (2) dust depletion; and (3) photoionization. At present, we believe the first two issues have relatively minor impact on derivations of  $N/\alpha$  and  $\alpha/H$  in the damped systems. In previous analyses and this work too, authors have relied on Si to serve as the  $\alpha$ -element because it is the most readily observed. This raises some concern because Si is expected to be synthesized in less massive progenitors of Type II SN than O or Mg (Woosley & Weaver 1995) and may even be substantially produced in Type Ia SN (Matteucci & Recchi 2001). Therefore, reporting  $[N/\alpha]$  as  $[N/\text{Si}]$  may complicate comparisons against theoretical models which generally reflect nucleosynthesis in the most massive stars. Empirically, however, we and others have found that  $[\text{O}/\text{Si}] \approx 0$  and  $[\text{S}/\text{Si}] \approx 0$  in the few damped systems where Si and O or S have been determined. Therefore, we believe the differ-

TABLE 13  
SUMMARY

QSO	$z_{abs}$	$N(\text{HI})$	$[\alpha/\text{H}]^a$	$[\text{N}/\alpha]$	IC <sup>c</sup>	Included	Ref
Q0000-2619	3.390	21.41	$-1.91 \pm 0.08$	$-0.74 \pm 0.04$	Y	Y	1,2,3
PH957	2.309	21.37	$-1.46^b \pm 0.08$	$-0.85 \pm 0.02$	Y	Y	4,5
Q0201+11	3.387	21.26	$-1.25^b \pm 0.15$	$-0.65 \pm 0.16$	?	Y	6
Q0201+36	2.463	20.38	$-0.41 \pm 0.05$	$> -0.94$	Y	Y	7,8
J0307-4945	4.468	20.67	$-1.55 \pm 0.12$		N	N	9
Q0336-01	3.062	21.20	$-1.41^b \pm 0.10$	$> -0.73$	Y	Y	8
Q0347-38	3.025	20.63	$-1.17 \pm 0.03$	$-0.54 \pm 0.04$	Y	Y	8, 10
HS0741+4741	3.017	20.48	$-1.69 \pm 0.10$	$-0.79 \pm 0.01$	Y	Y	8
Q0930+28	3.235	20.30	$-1.97 \pm 0.10$	$-0.56 \pm 0.02$	N	Y	8, 11
Q1055+46	3.317	20.34	$-1.65 \pm 0.15$	$< -0.57$	?	Y	11
BR1202-07	4.383	20.60	$-1.81 \pm 0.14$	$< -0.46$	?	Y	11
Q1223+17	2.466	21.50	$-1.59 \pm 0.10$	$-1.05 \pm 0.18$	N	N	8
Q1331+17	1.776	21.18	$-1.45 \pm 0.04$	$-0.49 \pm 0.11$	?	Y	5
Q1425+6039	2.827	20.30	$> -1.03$	$< -0.53$	N	N	8, 11
Q1759+75	2.625	20.76	$-0.89 \pm 0.01$	$-0.68 \pm 0.02$	N	Y	12
Q1946+7658	2.844	20.27	$-2.23 \pm 0.06$	$-1.43 \pm 0.04$	Y	Y	8, 11
Q2212-1626	3.662	20.20	$-1.90 \pm 0.08$	$< -0.69$	?	Y	11
BR2237-0607	4.080	20.52	$-1.87 \pm 0.11$	$< -0.34$	?	Y	11
HE2243-6031	2.330	20.67	$-0.87 \pm 0.03$	$-0.89 \pm 0.02$	?	Y	13
Q2343+12	2.431	20.34	$-0.54 \pm 0.10$	$-1.10 \pm 0.09$	N	N	5
Q2344+12	2.538	20.36	$-1.74 \pm 0.10$	$-0.81 \pm 0.03$	Y	Y	8
Q2348-14	2.279	20.56	$-1.92 \pm 0.08$	$< -1.38$	N	Y	2,8,14
QXO0001	3	20.70	$-1.81 \pm 0.05$	$-1.45 \pm 0.04$	Y	Y	8

<sup>a</sup>Assumes Si unless noted

<sup>b</sup>Sulfur

<sup>c</sup>See below for a detailed discussion of ionization corrections.

References. — Key to References – 1: Lu et al. (1996); 2: Prochaska & Wolfe (1999); 3: Molaro et al. (2000); 4: Wolfe et al. (1994); 5: Dessauges-Zavadsky, Prochaska, & D’Odorico (2002b); 6: Ellison et al. (2001); 7: Prochaska & Wolfe (1996); 8: This paper; 9: Dessauges-Zavadsky et al. (2001); 10: Levshakov et al. (2002); 11: Lu et al. (1998); 12: Prochaska et al. (2002); 13: Lopez et al. (2002); 14: Pettini et al. (1995)

ence between O and Si leads to an uncertainty in  $[N/\alpha]$  of less than 0.1 dex.

We expect that dust depletion has an even smaller effect on the  $[N/\alpha]$  and  $[\alpha/H]$  values than uncertainties between the various  $\alpha$ -elements. Although Si is significantly depleted along many ISM sightlines (e.g. Savage & Sembach 1996), the depletion levels in the damped Ly $\alpha$  systems (as inferred from Zn/Fe or S/Fe) are too small for the differential depletion of Si/N or Si/H to be important (e.g. Vladilo 1998). This is particularly true for the systems presented here where the Si/Zn and Si/S ratios are very nearly solar (Prochaska & Wolfe 2002; but see Ledoux et al. 2002 for a counter-example). The largest corrections one could derive for Si relative to N and H is +0.2 dex which would imply slightly lower  $N/\alpha$  ratios and a higher  $\alpha/H$  value.

The major sources of systematic error in converting  $N^0$ ,  $Si^+$ ,  $H^0$ , and  $O^0$  column densities into elemental abundances are ionization corrections. Consider first the ionization balance of  $O^0$ ,  $O^+$ ,  $N^0$ ,  $N^+$ ,  $H^0$ , and  $H^+$ . Charge-exchange reactions between ( $O^0$ ,  $H^0$ ) and ( $N^0$ ,  $H^0$ ) help to regulate the ionization fractions of these ions such that  $H^0/H \approx N^0/N \approx O^0/O$  when the volume density is large and the ionizing flux is modest. If the ratio of ionizing flux to volume density – the ionization parameter  $U$  – is large enough, then this set of equalities breaks down. Both  $O^0$  and  $N^0$  have larger cross-sections to photons with  $h\nu > 2$  Ryd than  $H^0$  (Sofia & Jenkins 1998) and these ions will be over-ionized:  $N^0/N < H^0/H$  and  $O^0/O < H^0/H$ . The likelihood of over-ionization for Ar is even greater as found in the Galactic ISM (Sofia & Jenkins 1998) and in damped systems (P02). In contrast,  $Si^+$  can be present in highly ionized regions such that  $Si^+/Si \geq H^0/H$  for nearly all physical conditions. The net result is that  $Si^+/H^0$  will overestimate Si/H and  $N^0/Si^+$  will underestimate N/Si *if ionization is significant* in the damped system, i.e., when  $\log U \gg -3$  (see below). The magnitude of these corrections ranges from a few hundredths dex in a very neutral gas to several tenths dex in an ionized gas. To accurately assess these ionization corrections, one must examine photoionization diagnostics within each damped system.

Historically, researchers have assumed that ionization corrections are negligible for the damped systems. This presumption is physically motivated by the very large optical depth at energies  $h\nu > 1$  Ryd implied by a sightline with  $N(HI) > 2 \times 10^{20} \text{ cm}^{-2}$  (Viegas 1994). Detailed theoretical models have drawn similar conclusions for the majority of elements observed in the damped systems (Howk & Sembach 1999; Vladilo et al. 2001). More recently, however, Prochaska et al. (2002) presented evidence for significant photoionization in  $\approx 50\%$  of the gas associated with the damped Ly $\alpha$  system at  $z = 2.62$  toward GB1759+75. For this gas, the ionization corrections are important for ions like  $N^0$  and  $Si^+$  relative to  $H^0$ . The correction for  $N^0/Si^+$  in this partially ionized gas is large:  $[N/\alpha] = [N^0/Si^+] + 0.3$  dex. Although the authors stress that this particular damped system has several characteristics which separate it from the majority of damped systems, its properties highlight the importance of assessing the ionization state of each damped system in order to convert the observed  $N^0/Si^+$ ,  $N^0/S^+$ ,  $O^0/H^0$ ,  $S^+/H^0$ , and  $Si^+/H^0$  ratios to  $N/\alpha$  and  $\alpha/H$ .

In Figure 11, we present a series of ionic ratios which qualitatively assess the level of ionization corrections for gas with a range of ionization states. These values were calculated with the CLOUDY software package (v95b; Ferland 2001) assuming a Haardt-Madau extragalactic background radiation field at  $z = 2.5$  (Haardt & Madau 1996). In panel (a) we plot  $N^0/Si^+$  and  $Si^+/H^0$  versus the ionization parameter,  $U \equiv \phi/(cn_H)$  where  $\phi$  is the surface flux of ionizing photons with  $h\nu > 1$  Ryd. The vertical dotted line at  $\log U = -3.5$  demarcates the transition from corrections of less than 0.2 dex for  $[N^0/Si^+]$  to greater than 0.2 dex. At this  $U$  value, panel (b) shows:  $[Fe^{++}/Fe^+] \approx -0.8$ ,  $[Si^{++}/Si^+] \approx -1.1$ ,  $[S^{++}/S^+] \approx -0.35$ ,  $[Ar^0/Si^+] \approx -0.7$ ,  $[Al^{++}/Al^+] \approx -0.6$ , and  $[N^+/N^0] \approx -0.5$ . Systems which exhibit significantly lower values for these ratios (higher values for  $Ar^0/Si^+$ ) should be predominantly neutral and require small corrections for  $[N/\alpha]$  and  $[\alpha/H]$ . Similarly, systems with larger values of these ratios are presumably partially ionized and may require significant ionization corrections. In the following sub-sections, we will describe the ionization diagnostics for each of the damped systems in the full nitrogen sample and evaluate the magnitude of ionization corrections.

### 3.1. Q0000–26, $z = 3.390$

Molaro et al. (2001) presented  $Ar^0$  measurements for this damped Ly $\alpha$  system which indicate a nearly solar Ar/Si ratio. We agree with their argument that the gas in this damped Ly $\alpha$  system is therefore predominantly neutral.

### 3.2. PH957, $z = 2.309$

Dessauges-Zavadsky, Prochaska, & D’Odorico (2002b) will present a detailed analysis of the photoionization state of this damped system. Their assessment, based on  $[Ar^0/S^+] \approx -0.2$  and observations of the Fe III 1122 transition, is that ionization corrections for  $N^0$  and  $S^+$  are small.

### 3.3. Q0201+11, $z = 3.387$

There is no photoionization diagnostic for this damped system, but we expect that its HI column density is large enough that photoionization corrections should be small.

### 3.4. Q0201+36, $z = 2.463$

Our new data on this system covers the Fe III 1122 transition and provides a measurement of  $Ar^0$ . The  $[Ar^0/Si^+]$  value of  $-0.42 \pm 0.1$  dex suggests the possibility of mild photoionization while the observed  $Fe^{++}/Fe^+$  ratio of  $-1$  dex indicates such effects are likely to be small. Altogether we expect ionization corrections of 0.1 dex or less and assume no correction. For this damped system, we measure ions for two  $\alpha$ -elements,  $Si^+$  and  $S^+$  whose abundances relative to solar are in reasonably good agreement. For  $[\alpha/H]$ , we adopt the  $[Si/H]$  value because the Si II 1808 profile is outside the Ly $\alpha$  forest and therefore less likely to be contaminated by line-blending.

### 3.5. J0307–4945, $z = 4.466$

Dessauges-Zavadsky et al. (2001) presented a detailed analysis of this damped system from their UVES observations which included measurements of N, Si, O and Fe

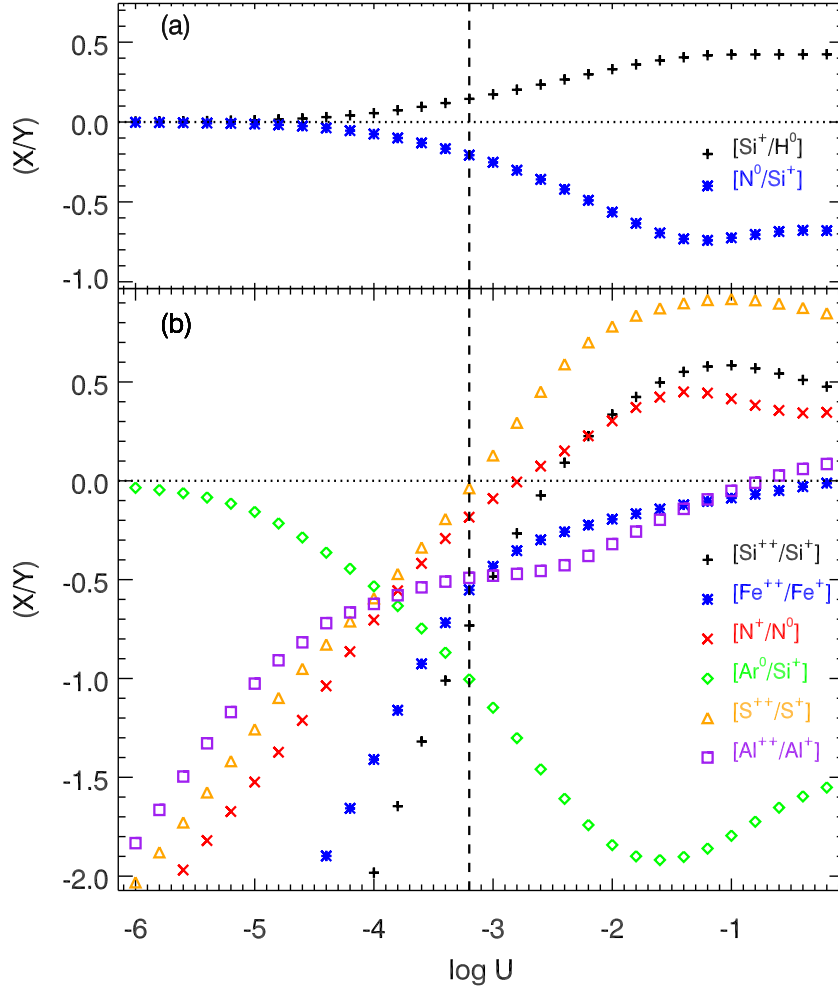


FIG. 11.— Ionic ratios predicted for a plane-parallel slab of gas with  $N(\text{HI}) = 10^{20} \text{cm}^{-2}$  for a range of ionization parameter  $U$ . These calculations were carried out with the CLOUDY software package. The dotted vertical line indicates the transition from a predominantly neutral gas where ionization corrections to  $[\text{N}^0/\text{Si}^+]$  are small to a partially ionized gas where ionization corrections are significant. Provided the appropriate observations, the calculations presented in this figure can be used to roughly assess the ionization corrections for a given damped  $\text{Ly}\alpha$  system.

among other elements. The authors presented  $\text{N}^0$  column density measurements for the strongest velocity components of this kinematically complex system and discussed the relatively low  $\text{N}/\alpha$  value. We are concerned, however, that this gas may require significant ionization corrections. We note that for those components where the O I profiles were unsaturated, the measured  $\text{O}^0/\text{Si}^+$  ratios are significantly sub-solar, in some cases by over 1 dex. This is a clear signature of photoionization in these weaker components where NI is undetected. Unfortunately, the O I profiles are heavily saturated in those components where NI was measured and it is impossible to accurately assess the photoionization state of the gas from the data presented in Dessauges-Zavadsky et al. (2001). Although we consider it a reasonable possibility that this system does exhibit a low  $\text{N}/\alpha$  value (consistent with the low nitrogen sub-sample discussed in § 4), we choose to eliminate it from our sample on the grounds that photoionization may be important.

### 3.6. Q0336–01, $z=3.062$

Our observations of the damped  $\text{Ly}\alpha$  system toward Q0336–01 provide a lower limit on the  $\text{Ar}^0/\text{S}^+$  ratio and place upper limits on the  $\text{N}^+/\text{N}^0$  and  $\text{Fe}^{++}/\text{Fe}^+$ . The nearly solar  $[\text{Ar}^0/\text{S}^+]$  ratio and the relatively small  $\text{N}^+/\text{N}^0$  and  $\text{Fe}^{++}/\text{Fe}^+$  limits all indicate this system is predominantly neutral.

### 3.7. Q0347–38, $z=3.025$

To assess the ionization state of this damped system we focus on the  $\text{Ar}^0$  measurements made by Levshakov et al. (2002). Their analysis indicates  $[\text{Ar}^0/\text{Si}^+] > -0.2$  implying this system is neutral. This conclusion is supported by our measured ratio of  $\text{Fe}^{++}/\text{Fe}^+ = -1.4$  dex which may be considered an upper limit (§ 2.4). We also report a  $\text{S}^{++}/\text{S}^+$  value of  $\lesssim -0.8$  dex which is consistent with this conclusion.

It is worth noting, that the C III 977, Fe III 1122, S III 1012, and Si III 1206 profiles all exhibit significant absorption at

$v > 20 \text{ km s}^{-1}$ . Although this absorption may result from coincident Ly $\alpha$  clouds, we contend the absorption is more likely due to a significantly ionized gas associated with the damped system. This component does not give rise to significant low-ion absorption, however, and therefore has no effect on our N/ $\alpha$  analysis.

### 3.8. *HS0741+47*, $z = 3.017$

Our spectrum of HS0741+47 includes coverage of several ionization diagnostics for this damped Ly $\alpha$  system including Ar I, Fe III, and N II transitions. Unfortunately, the Fe III 1122 and N II 1083 transitions appear to be blended with coincident Ly $\alpha$  forest clouds (Figure 4) and the resulting upper limits are not too meaningful. On the other hand,  $[\text{Ar}^0/\text{Si}^+] = -0.18$  and we contend the system is primarily neutral with ionization corrections for  $[\text{N}/\alpha]$  and  $[\alpha/\text{H}]$  less than 0.1 dex.

### 3.9. *Q0930+28*, $z = 3.235$

The strongest constraints on the ionization state of this system are the  $\text{N}^+/\text{N}^0$  and  $\text{Si}^{++}/\text{Si}^+$  ratios. The N II 1083 profile may be mildly blended with a coincident Ly $\alpha$  forest cloud, but we expect  $\text{N}^+/\text{N}^0 \approx -0.2$  dex which implies a modest ionization correction for nitrogen. Similarly, the saturated Si III 1206 profile yields a lower limit to  $\text{Si}^{++}/\text{Si}^+$  of  $-0.25$  dex consistent with this system being partially ionized. Altogether, we contend the N/ $\alpha$  and  $\alpha/\text{H}$  values would require significant ionization corrections and we do not include this system in our analysis. In passing, however, we note that the uncorrected  $[\text{N}/\alpha]$  and  $[\alpha/\text{H}]$  values are typical for the majority of our sample.

### 3.10. *Q1055+46*, $z = 3.317$

We have no ionization diagnostics for this system.

### 3.11. *BR1202-07*, $z = 4.383$

We have no ionization diagnostics for this system.

### 3.12. *Q1223+17*, $z = 2.466$

As described in § 2.7, we have been unable to measure an accurate  $\text{N}^0$  column density from our dataset and have not included this system. In passing, we note the Fe III and N II profiles indicate the gas is predominantly neutral at  $v \approx 0 \text{ km s}^{-1}$  but suggest the gas at  $v \approx -70 \text{ km s}^{-1}$  could be partially ionized. The latter point hinges on whether the feature observed at  $v \approx -70 \text{ km s}^{-1}$  in the Fe III 1122 profile is the result of a blend.

### 3.13. *Q1331+17*, $z = 1.776$

A complete analysis of this system's ionization state will be presented in Dessauges-Zavadsky, Prochaska, & D'Odorico (2002b). Their UVES observations of Fe III 1122 indicate the gas giving rise to the NI profiles is predominantly neutral.

### 3.14. *Q1425+60*, $z = 2.827$

This system exhibits several diagnostics which indicate photoionization is likely to be important. In particular, we find  $[\text{Ar}^0/\text{Si}^+] < -0.5$  dex and  $\text{N}^+/\text{N}^0 > 0$  dex. Although

the N II 1083 profile is mildly saturated and therefore resembles a typical Ly $\alpha$  cloud, we are confident it is not a coincident absorption line because the profile also exhibits a velocity component at  $v \approx -90 \text{ km s}^{-1}$  which coincides with a similar feature in the low-ion profiles. Analysing this single velocity component, we find  $\text{N}^+/\text{N}^0 \approx 0$  dex consistent with the total  $N(\text{N}^+)$  and  $N(\text{N}^0)$  values. Altogether we expect the measured  $\text{N}^0$  column density significantly underestimates the nitrogen elemental abundance. We choose to remove it from the analysis noting, however, that it does not appear to exhibit a low N/ $\alpha$  ratio. In fact, if ionization corrections to  $\text{N}^0$  and  $\text{Si}^+$  are significant, this system may exhibit a nearly solar N/ $\alpha$  ratio.

### 3.15. *GB1759+75*, $z = 2.625$

A detailed photoionization treatment of this damped system has been presented by P02. We concluded that roughly half of the gas is partially ionized with  $\text{N}^0/\text{Si}^+$  requiring significant ionization corrections. The remaining gas, meanwhile, is predominantly neutral. We are able to estimate the ionization corrections to  $[\text{N}/\alpha]$  and  $[\alpha/\text{H}]$  for the entire system and have therefore included it within our analysis. The corrections we adopt are  $+0.15$  dex to  $[\text{N}/\alpha]$  and  $-0.1$  dex to  $[\alpha/\text{H}]$  as measured from  $[\text{Si}/\text{H}]$ .

### 3.16. *Q1946+76*, $z = 2.844$

This well studied damped Ly $\alpha$  system has a relatively low HI column density and one of the lowest  $\text{N}^0/\text{Si}^+$  ratios observed. These factors raise concerns that its gas may be primarily ionized and that the low inferred N/ $\alpha$  value has resulted from photoionization. This concern is supported by the slightly sub-solar  $\text{O}^0/\text{Si}^+$  ratio, but we place a strict upper limit on  $\text{Si}^{++}/\text{Si}^+ < -0.75$  dex which suggests ionization corrections are not extreme. Unfortunately, the N II 1083 profile is blended and does not provide a useful limit on  $\text{N}^+/\text{N}^0$ . Nevertheless, the system may require an ionization correction for  $[\text{N}/\alpha]$  (see Figure 11) and we have remaining concerns on its ionization state. In the following, however, we proceed without adopting any correction.

### 3.17. *Q2212-16*, $z = 3.662$

There is no ionization diagnostic for this damped system.

### 3.18. *BR2237-06*, $z = 4.080$

There is no ionization diagnostic for this damped system.

### 3.19. *HE2243-60*, $z = 3.149$

This new damped Ly $\alpha$  system (Lopez et al. 2002) exhibits competing photoionization diagnostics. Although the system shows a significantly sub-solar  $\text{Ar}^0/\text{Si}^+$  ratio,  $[\text{Ar}^0/\text{Si}^+] = -0.5$ , Lopez et al. (2002) examined the  $\text{Al}^+$  and  $\text{Fe}^+$  column densities and argued that ionization corrections are likely to be small. We proceed under the assumption that ionization corrections to N/ $\alpha$  are small.

### 3.20. *Q2343+12*, $z = 2.431$

Dessauges-Zavadsky, Prochaska, & D'Odorico (2002b) will present a full analysis on the photoionization of this

system. We note here that they find a very low Ar<sup>0</sup>/Si<sup>+</sup> ratio and strong N<sup>+</sup> absorption indicating photoionization corrections will be important. As such, we have not included this system in our analysis.

### 3.21. *Q2344+12*, $z = 2.538$

Although our observations cover several ionization diagnostics, the only valuable ratio is Fe<sup>++</sup>/Fe<sup>+</sup>; N II 1083 is severely blended and the Ar<sup>0</sup> transitions provide only an upper limit to  $N(\text{Ar}^0)$ . The upper limit on Fe<sup>++</sup>/Fe<sup>+</sup> < -0.8 suggests the system is probably neutral but the N<sup>0</sup> and Si<sup>+</sup> column densities could be subject to small ( $\lesssim$  0.1 dex) ionization corrections. In the following, we adopt no corrections.

### 3.22. *Q2348-14*, $z = 2.279$

The very low upper limit on N<sup>0</sup>/Si<sup>+</sup> for this damped system raises concerns that photoionization may be important. Unfortunately, the existing spectra do not cover the Fe III or N II profiles. We do measure Al<sup>++</sup>/Al<sup>+</sup> = -0.55 dex but this diagnostic is relatively insensitive to the photoionization state (Figure 11) and does not provide a particularly meaningful constraint. We also place a lower limit on Si<sup>++</sup>/Si<sup>+</sup> of -0.7 dex which may be influenced by a line-blend in the Ly $\alpha$  forest. Unfortunately, these diagnostics are inconclusive. Most worrisome is the fact that the Si IV and C IV profiles exhibit significant features at essentially identical velocity as the low-ion absorption indicating ionized gas is at this velocity. As discussed in P02 and Wolfe & Prochaska (2000), it is unlikely that the gas responsible for the high-ion profiles is associated with the low-ion profiles in damped Ly $\alpha$  systems. Nevertheless, we have remaining concerns regarding the ionization state of this system. On the other hand, the N<sup>0</sup> column density is an upper limit and we are reasonably confident that the N/ $\alpha$  is very low in this damped system.

### 3.23. *QXO0001*, $z = 3$

Although our observations provide several ionization diagnostics for this system, it is difficult to draw a definite conclusion on its ionization state. The N II 1083 profile is blended and places a large upper limit on N<sup>+</sup>/N<sup>0</sup>. The Ar I transition is also blended and provides an upper limit [Ar<sup>0</sup>/Si<sup>+</sup>] < 0 dex which is consistent with both a neutral and ionized gas. Meanwhile, the partially saturated Si III 1206 transition implies Si<sup>++</sup>/Si<sup>+</sup>  $\gtrsim$  -1 and we place an upper limit on Fe<sup>++</sup>/Fe<sup>+</sup> of -1 dex. These latter two diagnostics suggest the system is primarily neutral, but a mild ionization correction to N/ $\alpha$  is allowed (up to 0.2 dex). We proceed assuming a +0.1 dex correction to [N/ $\alpha$ ] and no correction to [ $\alpha$ /H].

## 4. ANALYSIS AND DISCUSSION

### 4.1. *What The Data Reveal*

Abundance results from Table 13 are presented graphically in Figure 12. This figure shows the abundance ratios [N/ $\alpha$ ] versus [ $\alpha$ /H] for a large sample of H II regions and blue compact galaxies compiled by Henry & Worthey (see their Figure 6 along with the caption, which identifies the numerous data sources). To their sample we have now

added our DLA results, which are shown in the figure with open circles, triangles (limits), and error bars.

The quantity [ $\alpha$ /H] in the figure is a gauge of metallicity and refers to those heavy elements which are produced through subsequent additions of alpha nuclei. In the case of the Henry & Worthey sample,  $\alpha$  corresponds to oxygen, while for the objects in our sample, it refers to silicon in most cases, and sulfur in a few cases (Table 13). Metallicity is in turn a measure of the extent to which the observed gas, which presumably began as pristine and metal-poor in these objects, has been processed through stars, since metal abundances rise as nuclear products from evolved stars are added to the gas. Metallicity is directly related to the total amount of star formation occurring since the system formed, and therefore values increase with time with a slope determined by the star formation rate and are tempered by the accretion of primordial gas from the surrounding IGM. On the other hand, [N/ $\alpha$ ] measures the differential change in nitrogen relative to  $\alpha$ -elements as processing goes forward. It is sensitive to the stellar yields for each element as well as the form of the initial mass function, but relatively insensitive to the detailed history of the star formation rate.

As we study the global pattern created by the emission line objects in Figure 12, we identify a lower-bound envelope behind which points are concentrated in number densities that fall off with increasing distance from the envelope. Referring to the discussion in § 1, the plateau in the envelope at low metallicity that is displayed by the metal-poor galaxies (Izotov & Thuan 1999; Kobulnicky & Skillman 1996) is explained by the dominance of primary (metal-insensitive) nitrogen production at low metallicity. Likewise, the upturn at higher metallicities can be attributed to increasing contributions from secondary (metal-sensitive) production. Currently, the causes of the scatter behind the envelope are not well-understood, although several theories have been proposed (Garnett 1990; Pilyugin 1993).

Most of the data points in Figure 12 collectively represent emission line regions in many different host galaxies of several different galaxy morphologies. Therefore, the fact that we see a pattern formed by this diverse group of objects suggests that, to first order, universal synthesis patterns of stars, as communicated to the environment through their IMF-weighted yields, are more important than local factors such as the star formation rate, infall, outflow, etc. for determining how nitrogen and  $\alpha$ -element abundances evolve with respect to each other.

Now consider the damped Ly $\alpha$  systems plotted in Figure 12. The majority follow a lower metallicity extension of the N/ $\alpha$  plateau expressed by the emission line regions, and unlike previous studies (e.g. L98), we observe minimal scatter in this group. The DLA 'plateau' values exhibit an *rms* scatter < 0.2 dex which is remarkably small given the systematic uncertainties described in § 3. Furthermore, all of the limits in this sub-sample are consistent with an [N/ $\alpha$ ] value of -0.75 dex. In contrast with the emission line regions, we identify three low nitrogen damped systems (LN-DLA) which represent a region of the plot that is isolated from and discontinuous with the main pattern. Similar to the major DLA population, these LN-DLA also exhibit minimal dispersion in their N/ $\alpha$  values. Therefore,



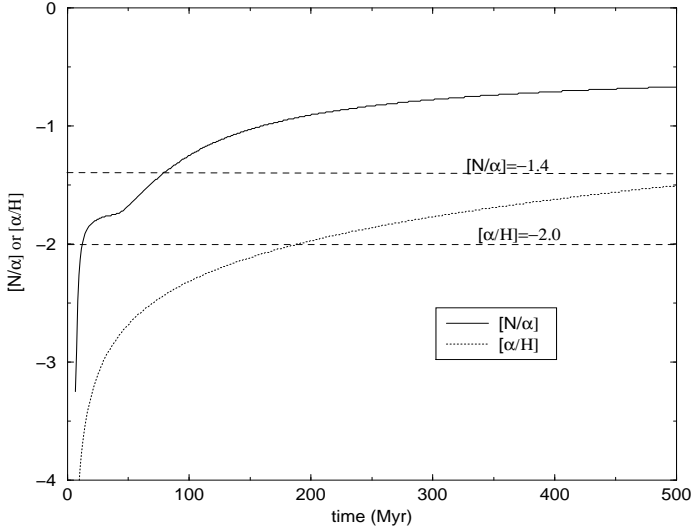


FIG. 13.—  $[\text{N}/\alpha]$  (solid curve) and  $[\alpha/\text{H}]$  (dotted curve) versus time in Myr for model B of HEK00. The horizontal dashed lines indicate centroid values for observed  $[\text{N}/\alpha]$  and  $[\alpha/\text{H}]$  associated with the LN-DLA objects displayed in Figure 12.

250 Myr<sup>5</sup>. The challenge for this scenario is revealed by Figure 13 which plots  $[\text{N}/\alpha]$  and  $[\alpha/\text{H}]$  versus time in Myr for model B of HEK00, the model which passes nearest the location of the LN-DLAs. Overplotted on the theoretical curves are the  $\text{N}/\alpha$  and  $\alpha/\text{H}$  values (horizontal dashed lines) of the LN-DLA sample. The plots show that the required levels are not reached at the same time:  $[\text{N}/\alpha]$  reaches a level of  $-1.4$  at the same time that  $[\alpha/\text{H}]$  is about 0.5 below  $-2.0$  dex. This inconsistency could be overcome, however, by fine-tuning the star formation efficiency. More important is that model B and its variants predict the gas will spend as much time at  $[\text{N}/\alpha] \approx -1.4$  as it will at  $-1.2$ ,  $-1.6$  dex, and other low values. Therefore, one would expect the LN-DLA to uniformly fill the region below the higher  $\text{N}/\alpha$  plateau expressed by the majority of DLA. The identification of the three LN-DLA at nearly the same  $\text{N}/\alpha$  value must be explained as a coincidence, i.e., this scenario cannot naturally reproduce a bimodal distribution.

In considering option 2 above, we employ a simple closed-box model of chemical evolution in order to estimate the ratio of nitrogen to oxygen yields needed to explain the observed  $[\text{N}/\alpha]$  of  $-1.4$  of the LN-DLA. Recall that the metallicity in a simple model can be expressed as  $Z_x = -y_x \ln \mu$ , where  $Z_x$  is the mass fraction of element  $x$ ,  $y_x$  is the total yield of a population of stars characterized by a Salpeter IMF per unit of stellar material forever locked up in remnants, and  $\mu$  is the gas fraction (Tinsley 1980). From the above observed value of  $[\text{N}/\alpha]$  and the solar value for  $\text{N}/\text{O}$  of  $-0.9$  (Grevesse & Noels 1996) we infer that  $Z_{\text{N}}/Z_{\text{O}} = y_{\text{N}}/y_{\text{O}} = 0.005$ . HEK00 integrated several sets of published yields over a Salpeter IMF, and we can now compare their results for low metallicity directly with

<sup>5</sup> Siess, Livio, & Lattanzio (2002) have recently calculated IMS evolution models in which they find that the stellar mass threshold for N production drops at lower metallicity, thus increasing the timescale for its production by IMS even further.

this observed value. Such a comparison shows that current published yield predictions of  $\text{N}/\text{O}$  are about two orders of magnitude above the level implied by the LN-DLA observations. Their results appear to rule out option 2 above, although published IMS yield calculations so far do not extend down to metallicities below 0.001. Furthermore, there is no indication from published IMS nitrogen yields that they are highly sensitive to metallicity (van den Hoek & Groenewegen 1997; Marigo 2001). Finally, it would be very difficult to explain the bimodality of  $[\text{N}/\alpha]$  values at the same  $[\alpha/\text{H}]$  metallicity in this scenario.

For option 3 we compare in a similar way the same simple model results to predicted yield ratios. Heger & Woosley (2002) have calculated models of massive Pop III stars ranging in mass from 140 to 260  $M_{\odot}$  and predicted yields for  $^{14}\text{N}$  and  $^{16}\text{O}$ . Simply by inspecting their results we can see that values of  $\text{N}/\text{O}$  resulting from their models range from about  $10^{-6}$  in the least massive stars to  $10^{-7}$  in the most massive ones. In addition, Woosley & Weaver (1995) predict N and O production by zero metallicity stars between 12-40  $M_{\odot}$  and find values of  $\text{N}/\text{O}$  of a few times  $10^{-4}$ , where again we have used the HEK00 results for yields integrated over a Salpeter IMF for comparison. These values are lower than necessary to explain LN-DLAs. However, in their Population III stellar models Umeda, Nomoto, & Nakamura (2000) predict  $^{14}\text{N}/^{24}\text{Mg}$  values of roughly 1/4 solar, which they say implies a large contribution of Population III stars to the early nitrogen buildup in their yield ratios which are consistent with these. In summary, while the relevance of Population III stars is presently unclear, these stars could ultimately prove important for the issue of early nitrogen production. Furthermore, if one could introduce a Pop III model which reproduced the observed LN-DLA population, it could reasonably account for the bimodal distribution where the higher  $\text{N}/\alpha$  DLA represent a second generation of star formation.

For the remainder of the discussion, we explore the fourth hypothesis: star formation is either characterized by (1) a top-heavy initial mass function at early times and/or low metallicities, such that there is a relative deficiency of IMS; or (2) a stellar population that is truncated below a certain mass threshold. In either case, the observed  $[\text{N}/\alpha]$  in the LN-DLAs is dominated by the yield patterns of massive stars.

To test this hypothesis, we employ the numerical code of HEK00 and calculate two types of chemical evolution models, both of which assume a closed system, i.e. no matter exchange with the environment. In the first set of models we ignore evolutionary time lags among stars of different progenitor masses (instantaneous recycling approximation), while in the second set we relax this assumption. Otherwise the model types are identical. The numerical code we employed is described in detail in HEK00. The only alterations we made relate to the star formation rate (eq. 18 in HEK00), where we used 1.5 rather than 2.0 for the exponent and set the efficiency factor to a constant value of 0.003 throughout.

We tested two sets of yields comprising the following combinations: (1) Woosley & Weaver (1995; massive stars) and van den Hoek & Groenewegen (1997; IMS); and (2) Portinari et al. (1998; massive stars) and Marigo (2001; IMS).

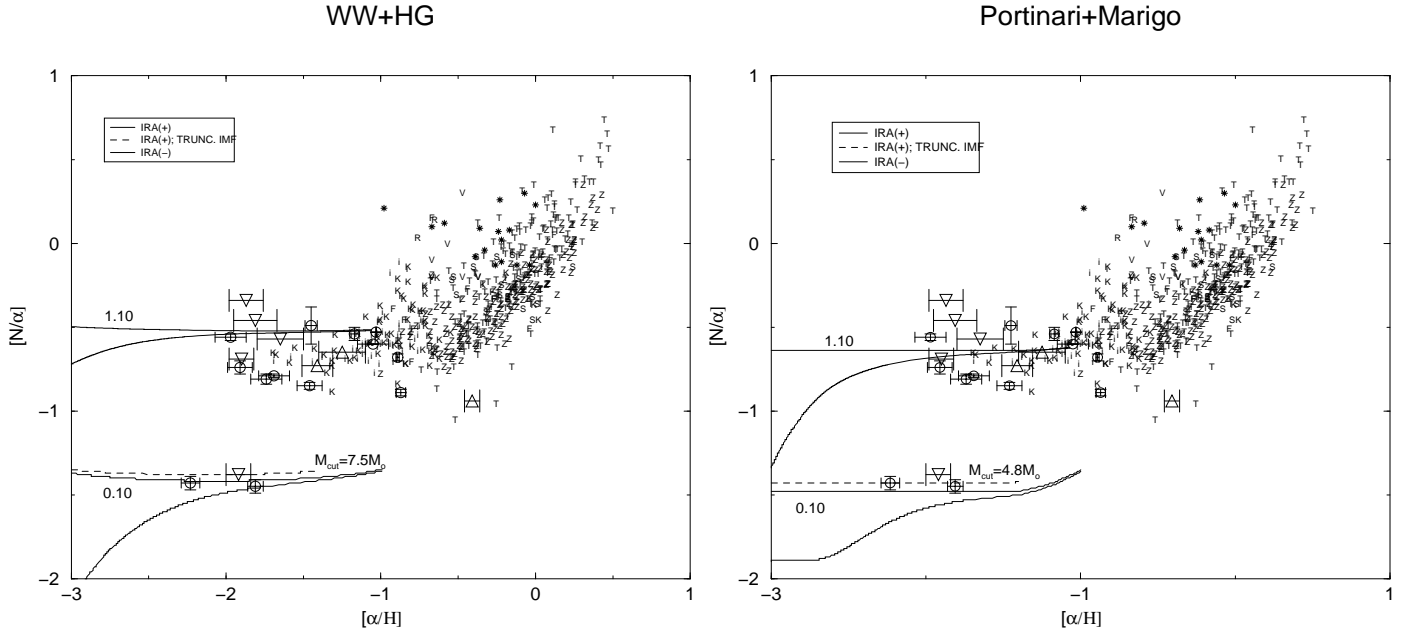


FIG. 14.— (a) Model results for set 1 stellar yields displayed with data points of Figure 12. Light solid curves represent results for the two different IMF slopes indicated and when instantaneous recycling is assumed (IRA+). Heavy solid lines show tracks for same models except that the instantaneous recycling assumption is relaxed (IRA-). The dashed line shows the model result when the IMF is truncated below  $7.5 M_{\odot}$  and instantaneous recycling is assumed. (b) Same as (a) but for set 2 stellar yields.

Our calculations, therefore, accounted for the effects of progenitor mass and metallicity on the yields. The IMF was taken to be a power law form, the index of which we varied so as to alter the relative mix of massive stars and IMS. For the models which assumed instantaneous recycling, we calculated an additional model subset for each yield set using a Salpeter IMF (index=1.35) and experimented with different lower mass threshold values until finding one which satisfactorily reproduced the observed  $[N/\alpha]$  value. Besides the choice of yield set, the only parameters allowed to change in our models were the slope and lower mass threshold of the IMF.

The model results assuming instantaneous recycling are shown with solid lines in Figures 14a,b, where each graph represents models associated with one yield set (see figure legends for line-type definitions). Lines are labeled according to IMF slope or cutoff mass<sup>6</sup>. Because of the instantaneous recycling assumption, no time lag exists between IMS and massive star release of N into the interstellar medium, and thus the tracks for these models are horizontal lines. In Figure 14a, where we employed the set (1) yields, the positions of the three LN-DLAs are consistent with a system whose stellar population possessed a top-heavy IMF with a slope of roughly 0.10 or with a Salpeter IMF but truncated below  $7.5 M_{\odot}$ . In Figure 14b, using set (2) yields, the LN-DLAs are again consistent with an IMF slope of 0.10 or a mass cutoff of  $4.8 M_{\odot}$ . Note that for each yield set a slope of 1.10 produces reasonable fits to the plateau region for both yield sets<sup>7</sup>. Finally, we point

<sup>6</sup> Note that because we are only interested in the results at low metallicity, all models were stopped when  $[\alpha/H] = -1$ .

<sup>7</sup> The difference here between 1.10 and 1.35 (Salpeter slope) is not of immediate concern, since uncertainties in the yields themselves are roughly a factor of two.

out that  $[N/\alpha]$  is quite sensitive to the value of the mass cutoff in both cases, since it falls within the mass range where most IMS N is produced in both cases.

Results for models without the instantaneous recycling approximation are shown with bold lines. The IMF slope in each case is identical to the model track with which the bold line merges close to  $[\alpha/H] = -1$ . The gradual rise in  $[N/\alpha]$  with metallicity for these models is simply due to the delayed contribution of IMS to the N buildup. Clearly, these models are still capable of reproducing DLA observations for both the plateau and LN-DLA objects.

Thus, our closed box models, calculated using two different sets of theoretical stellar yields, appear to be consistent with the idea that LN-DLAs are systems which have evolved with either top-heavy or truncated IMFs. We find a representative IMF slope of 0.10 or a mass cutoff of  $4.8 M_{\odot}$  with yield set (1) and  $7.5 M_{\odot}$  with yield set (2). This conclusion holds regardless of whether instantaneous recycling is assumed. The reason that the altered IMF slope or the truncation can explain the LN-DLAs is simply that the relative contribution of IMS to nitrogen evolution is significantly reduced, leaving the massive stars to dominate the production of both nitrogen and oxygen.

The top-heavy IMF hypothesis, we believe, offers a viable alternative to ones already suggested by others and briefly discussed above. Furthermore, this scenario may also explain the bimodal distribution observed for the DLA measurements (see below). *Indeed, the LN-DLAs may offer the first evidence that the mass spectra of some early stellar populations were much different than we observe today.*

There is currently no convincing evidence for the existence, past or present, of an IMF which differs markedly from those derived from observations in local systems such

as the form presented by Scalo (1986). Instead, most evidence points to the IMF being invariant (e.g. Kroupa 2001) in space and time. However, simple arguments based upon a Jeans mass analysis imply that at low metallicities, star formation should favor higher mass objects. This factor alone alerts us to a potential top-heavy IMF (THIMF) at early times.

Silk (1998) discusses several observations which may suggest a THIMF at very early epochs, although he is very careful to note that they are all circumstantial and in no way clinches the case for a THIMF. Theoretical support for a THIMF comes from the models of Nakamura & Umemura (2001; 2002), who study star formation in extremely metal-deficient protogalactic environments and predict a resulting bimodal IMF with peaks around 1 and 100  $M_{\odot}$ .

At present, we favor the THIMF interpretation because it accurately reproduces the  $N/\alpha$  values of the LN-DLA and because it may be consistent with a bimodal distribution. The latter point would hold if a primordial THIMF abruptly changed over to the form we observe today after a certain threshold was passed. Bromm et al. (2001) have experimented with numerical simulations of the collapse of pre-enriched primordial objects and set a value of  $Z_{crit} = 5 \times 10^{-4} Z_{\odot}$  as the metallicity threshold when this changeover occurs (see also Abel, Bryan, & Norman 2000). In the end it seems likely that measurements of integrated light from early systems will prove useful in deciding between the THIMF option and the other possibilities which are all consistent with a normal stellar mass spectrum.

## 5. SUMMARY AND CONCLUDING REMARKS

In this paper we presented  $N/\alpha$  vs.  $\alpha/H$  measurements of a moderate sample of damped Ly $\alpha$  systems and identified a possible bimodality in the  $N/\alpha$  values at the lowest metallicity. While the majority of low metallicity DLA have  $N/\alpha$  values consistent with low metallicity emission-line regions in the local universe, a sub-sample exhibits significantly lower  $N/\alpha$  values (the LN-DLA). Unlike previous works, we found minimal scatter among the members of each of the sub-samples and therefore argue that the DLA measurements form a bimodal distribution. We considered several scenarios which could account for these observations: (1) these systems are too young ( $< 250$  Myr) for their intermediate-mass stars to have produced N; (2) a reduced production of N in intermediate-mass stars at low metallicity; (3) Population III nucleosynthesis; and (4) chemical evolution with a top-heavy IMF. Currently, we do not favor the first three scenarios. If the LN-DLA are to be explained through the young age of the absorbing galaxy, then one would expect the LN-DLA to fill the parameter space beneath the plateau instead of comprising a bimodal distribution. Regarding the second option, it would be difficult to explain why DLA with the same metallicity exhibit such different  $N/\alpha$  values. Finally, the third avenue is promising but current models (e.g. Heger & Woosley 2002) of Pop III nucleosynthesis appear to underpredict the  $N/\alpha$  levels observed in the damped systems.

Therefore, we favor a scenario where the LN-DLA were enriched with an initial starburst with suppressed formation of intermediate-mass stars. We found that a starburst characterized by a power-law IMF with slope 0.10 or a

mass cut of  $\approx 5 - 8 M_{\odot}$  would successfully reproduce the observed LN-DLA values. This scenario allows for the bimodal DLA distribution of  $N/\alpha$  without requiring that we have observed the damped systems at a special moment in time. Furthermore, an initial burst of star formation in a low metallicity environment may suppress the formation of lower mass stars (e.g. Abel, Bryan, & Norman 2000; Bromm et al. 2001) and naturally lend to a bimodal distribution.

Before concluding, we wish to briefly comment on correlations between  $N/\alpha$  and other physical properties of the damped Ly $\alpha$  systems. In terms of kinematic characteristics, two of the LN-DLA systems (Q1946+75,  $z=2.8$ ; Q2348-14,  $z=2.3$ ) have among the simplest kinematics of any damped Ly $\alpha$  system. This may suggest these systems have particularly small mass and/or relatively quiescent star formation. We note, however, that several other systems with higher  $N/\alpha$  ratios also exhibit very simple kinematics. The only other trend we can identify is an increase in  $N/\alpha$  with increasing  $z_{abs}$  which is contrary to expectation. Perhaps this absence of correlation is further evidence that the production of N is largely independent of environment and star formation history as suggested by the uniformity of the emission line sample.

The authors wish to recognize and acknowledge the very significant cultural role and reverence that the summit of Mauna Kea has always had within the indigenous Hawaiian community. We are most fortunate to have the opportunity to conduct observations from this mountain. We thank the Keck staff who were instrumental in acquiring this data. We also thank Max Pettini and Sara Ellison for their helpful comments. We also acknowledge the construction of the MAKEE software package by Tom Barlow. Finally, we thank Gary Ferland and CLOUDY associates for the CLOUDY software package. This work was partially supported by NASA through a Hubble Fellowship grant HF-01142.01-A awarded by STScI to JXP. RBCH was partially supported by NSF grant AST-9819123. The work of DT, NS, JMO, and DK was funded in part by grant NASA funds G-NASA/NAG5-3237 and NAG5-9224, and by NSF grant AST-9900842. AMW was partially supported by NSF grant AST 0071257.

## REFERENCES

- Abel, T., Bryan, G.L., & Norman, M.L. 2000, *ApJ*, 540, 39
- Alcock, C., et al. 2000, *ApJ*, 542, 281
- Bergeson, S.D. & Lawler, J.E. 1993, *ApJ*, 414, L137
- Bromm, V., Ferrara, A., Coppi, P.S., & Larson, R.B. 2001, *MNRAS*, 328, 969
- Carretta, E., Gratton, R. G., & Sneden, C. 2000, *A&A*, 356, 238
- Centurión, M., Bonifacio, P., Molaro, P., & Vladilo, G. 1998, *ApJ*, 509, 620
- Clayton, D.D. 1983, *Principles of Stellar Evolution and Nucleosynthesis* (New Haven, CT: Yale Univ. Press)
- Cowley, C.R. 1995, *Cosmochemistry* (Cambridge: Cambridge Univ. Press)
- Dekker, H., D'Odorico, S., Kaufer, A., Delabre, B., & Kotzlowski, H. 2000, *SPiE*, 4008, 534
- Dessauges-Zavadsky, M., D'Odorico, S., McMahon, R.G., Molaro, P., Ledoux, C., Péroux, C., & Storríe-Lombardi, L.J. 2001, *A&A*, 370, 426
- Dessauges-Zavadsky, M., Prochaska, J.X., & D'Odorico, S. 2002a, *A&A*, submitted
- Dessauges-Zavadsky, M., Prochaska, J.X., & D'Odorico, S. 2002b, *A&A*, in prep
- Ellison, S.L., Pettini, M., Steidel, C.C., & Shapely, A.E. *ApJ*, 549, 770
- Ferland, G. J. 2001, *PASP*, 113, 41
- Garnett, D.R. 1990, *ApJ*, 363, 142
- Grevesse, N., Noels, A., & Sauval, A.J. 1996, In: *Cosmic Abundances*, S. Holt and G. Sonneborn (eds.), *ASPCS*, V. 99, (BookCrafters: San Francisco), p. 117
- Haardt, F. & Madau, P. 1996, *ApJ*, 461, 20
- Heger & Woosley, S. 2002, *ApJ*, 567, 532
- Henry, R.B.C., Edmunds, M.G., & Köppen, J. 2000, *ApJ*, 541, 660 (HEK00)
- Henry, R.B.C., Kwitter, K.B., & Bates, J.A. 2000, *ApJ*, 531, 928
- Henry, R.B.C. & Worthey, G. 1999, *PASP*, 111, 919
- van den Hoek, L.B., & Groenewegen, M.A.T. 1997, *A&A*, 123, 305
- Holweger, H. 2001, in *Solar and Galactic Composition*, ed. R.F. Wimmer-Schweingruber, (Berlin: Springer), 23
- Howk, J.C. & Sembach, K.R. 1999, *ApJ*, 523, 141L
- Howk, J.C., Sembach, K.R., Roth, K.C., & Kruk, J.W. 2000, *ApJ*, 544, 867
- Izotov, Y.L., & Thuan, T.X. 1999, *ApJ*, 511, 639
- Kirkman, D. & Tytler, D. 1997, *ApJ*, 484, 672
- Kobulnicky, H.A. & Skillman, E.D. 1996, *ApJ*, 471, 211
- Kroupa, P. 2001, *MNRAS*, 322, 231
- Ledoux, C., Bergeron, J., & Petitjean, P. 2002, *A&A*, in press (astro-ph/0202134)
- Levshakov, S.A., Dessauges-Zavadsky, M., D'Odorico, S., & Molaro, P. 2002, *ApJ*, in press (astro-ph/0105529)
- Lopez, S., Reimers, D., D'Odorico, S., & Prochaska, J.X. 2002, *A&A*, in press (astro-ph/0202036)
- Lu, L., Sargent, W.L.W., Barlow, T.A., Churchill, C.W., & Vogt, S. 1996, *ApJS*, 107, 475
- Lu, L., Sargent, W.L.W., & Barlow, T.A. 1997, astro-ph/9711298
- Lu, L., Sargent, W.L.W., & Barlow, T.A. 1998, *AJ*, 115, 55
- Maeder, A. 1992, *A&A*, 264, 105
- Marigo, P. 2001, *A&A*, 370, 194
- Matteucci, F. & Recchi, S. 2001, *ApJ*, 558, 351
- McWilliam, A., Preston, G.W., Sneden, C., & Searle, L. 1995, *AJ*, 109, 2757
- McWilliam, A. 1997, *ARA&A*, 35, 503
- Molaro, P., Bonifacio, P., Centurión, M., D'Odorico, S., Vladilo, G., Santin, P., & Di Marcantonio, P. 2000, *ApJ*, 541, 54
- Molaro, P. et al. 2001, *ApJ*, in press
- Morton, D.C. 1991, *ApJS*, 77, 119
- Morton, D.C. 2002, in prep
- Pei, Y.C., Fall, S.M., & Hauser, M.G. 1999, *ApJ*, 522, 604
- Péroux, C., Storríe-Lombardi, L.J., McMahon, R.G., Irwin, M., & Hook, I.M. 2001, *AJ*, 121, 1799
- Pettini, M., Smith, L. J., Hunstead, R. W., and King, D. L. 1994, *ApJ*, 426, 79
- Pettini, M., Lipman, K., & Hunstead, R.W. 1995, *ApJ*, 451, 100
- Pettini, M., Ellison, S., Bergeron, J., & Petitjean, P. 2002, *A&A*, in press (astro-ph/0205472)
- Pilyugin, L.S. 1993, *A&A*, 277, 42
- Portinari, L., Chiosi, C., & Bressan, A. 1998, *A&A*, 334, 505
- Prochaska, J. X. & Wolfe, A. M. 1996, *ApJ*, 470, 403 (PW96)
- Prochaska, J. X. & Wolfe, A. M. 1997, *ApJ*, 474, 140
- Prochaska, J. X. & Wolfe, A. M. 1997, *ApJ*, 486, 73
- Prochaska, J. X. & Wolfe, A. M. 1999, *ApJS*, 121, 369 (PW99)
- Prochaska, J.X. & Wolfe, A.M., 2000, *ApJ*, 533, L5 (PW00)
- Prochaska, J. X., Naumov, S.O., Carney, B.W., McWilliam, A., & Wolfe, A.M. 2000, *AJ*, 120, 2513 (P00)
- Prochaska, J.X., et al. 2001, *ApJS*, 137, 21
- Prochaska, J.X. & Wolfe, A.M. 2002, *ApJ*, 566, 68
- Prochaska, J.X., Howk, J.C., O'Meara, J.M., Tytler, D., Wolfe, A.M., Kirkman, D., Lubin, D., & Suzuki, N. 2002, *ApJ*, in press
- Salpeter, E.E. 1955, *ApJ*, 121, 161
- Savage, B. D. and Sembach, K. R. 1991, *ApJ*, 379, 245
- Savage, B. D. & Sembach, K. R. 1996, *ARA&A*, 34, 279
- Scalo, J. 1986, *Fund. Cos. Phys.*, 11, 1
- Siess, L., Livio, M., & Lattanzio, J. 2002, *ApJ*, in press, astro-ph/0201284
- Silk, J. 1998, in *The Stellar Initial Mass Function*, *ASP Conf. Ser.*, 142, eds. Gilmore, G., & Howell, D. (San Francisco: ASP) p177
- Sofia, U.J. & Jenkins, E.B. 1998, *ApJ*, 499, 951
- Storríe-Lombardi, L.J. & Wolfe, A.M. 2000, *ApJ*, 543, 552
- Tinsley, B.M. 1979, *ApJ*, 229, 1046
- Tripp, T. M., Lu L., & Savage B.D. 1996, *ApJS*, 102, 239
- Umeda, H., Nomoto, K., & Nakamura, T. 2000, in "The First Stars", ed. A. Weiss, T. Abel, & V. Hill, (Springer, Heidelberg)
- Umeda, H. & Nomoto, K. 2001, *ApJ*, submitted (astro-ph/0103241)
- Viegas, S.M. 1994, *MNRAS*, 276, 268
- Vladilo, G. 1998, *ApJ*, 493, 583
- Vladilo, G., Centurión, M., Bonifacio, P., & Howk, J.C. 2001, *ApJ*, 557, 1007
- Vogt, S.S., Allen, S.L., Bigelow, B.C., Bresee, L., Brown, B., et al. 1994, *SPiE*, 2198, 362
- Wheeler, J.C., Sneden, C., & Truran, J.W.Jr. 1989, *ARA & A*, 27, 279
- Wolfe, A. M., Fan, X.-M., Tytler, D., Vogt, S. S., Keane, M. J., & Lanzetta, K. M. 1994, *ApJ*, 435, L101
- Wolfe, A. M., Lanzetta, K. M., Foltz, C. B., and Chaffee, F. H. 1995, *ApJ*, 454, 698
- Wolfe, A. M. & Prochaska, J.X. 2000a, *ApJ*, 545, 591
- Woosley, S.E. & Weaver, T.A. 1995, *ApJS*, 101, 181